Orientational correlations and entropy in liquid water

Themis Lazaridis
Department of Chemistry, Harvard University, Cambridge, Massachusetts 02138

Martin Karplus
Department of Chemistry, Harvard University, Cambridge, Massachusetts and Laboratoire de Modelisation et Simulation Moléculaires, Institut le Bel, Université Louis Pasteur, 67000 Strasborg, France

(Received 29 January 1996; accepted 17 May 1996)

The molecular pair correlation function in water is a function of a distance and five angles. It is here separated into the radial distribution function (RDF), which is only a function of distance, and an orientational distribution function (ODF), which is a function of the five angles for each distance between the molecules. While the RDF can be obtained from computer simulations, this is not practical for the ODF due to its high dimensionality. Two approaches for obtaining an approximation to the ODF are introduced. The first uses a product of one- and two-dimensional marginal distributions from computer simulations. The second uses the gas-phase low-density limit as a reference and applies corrections based on (a) the orientationally averaged interactions in the liquid calculated by simulations, and (b) the observed differences in the one- and two-dimensional marginal distributions in the gas and in the liquid. The site superposition approximation was also tested and found to be inadequate for reproducing the orientationally averaged interaction energy and the angular distributions obtained from the simulations. The two approximations to the pair correlation function are employed to estimate the contribution of two-particle correlations to the excess entropy of TIP4P water. The calculated value is comparable to the excess entropy of TIP4P water estimated by other methods and to the experimental excess entropy of liquid water. More than 90% of the orientational part of the excess entropy is due to correlations between first neighbors. The change in excess entropy with temperature gives a value for the heat capacity that agrees within statistical uncertainty with that obtained from the change in energy with temperature and is reasonably close to the experimental value for water. The effect of pressure on the entropy was examined and it was found that increase in the pressure (density) causes a *reduction* of orientational correlations, in agreement with the idea of pressure as a ''structure breaker'' in water. The approach described here provides insight concerning the nature of the contributions to the excess entropy of water and should be applicable to other simple molecular fluids. © *1996 American Institute of Physics.* [S0021-9606(96)51532-1]

I. INTRODUCTION

The structure of liquid water has been a subject of intense interest for many decades. Bernal and Fowler[1] first described water as a locally tetrahedral network of hydrogen bonded molecules lacking long range order and proposed a simple model for the water molecule. Since then, much effort has been devoted to finding phenomenological models that explain the anomalous thermodynamic and kinetic properties of the liquid, such as its density maximum and the expansion upon freezing, the isothermal compressibility minimum at 46 °C, the high heat capacity, and the decrease of viscosity with pressure.[2] The models fall into two classes. The first envision water as a mixture of two or more ''species'' with different coordination, enthalpy, and entropy.[3,4] The anomalies are then explained by a change in the mole fraction of these species with temperature or pressure. The second class of models view water as a random network of hydrogen-bonded water molecules lacking long range order due to the presence of restricted bending of the hydrogen bonds.[5–7]

A more fundamental approach to the structure of water or other molecular fluids makes use of the N-body correlation function[8,9]

$$g^{(N)}(\mathbf{r}^N,\omega^N)$$

which is a function of the positions and orientations of all the molecules in the fluid. This function, even if it were possible to calculate it theoretically, is too complex to visualize as a basis for obtaining physical insights. An alternative approach describes the structure of a fluid by a series of correlation functions of increasing complexity

$$g^{(2)}(\mathbf{r}^2,\omega^2),\quad \delta g^{(3)}(\mathbf{r}^3,\omega^3),\quad \delta g^{(4)}(\mathbf{r}^4,\omega^4),\quad \cdots,$$

where $g^{(2)}$ is the pair correlation function (PCF) and $\delta g^{(3)}$, for example, is defined by the equation

$$g^{(3)}(\mathbf{r}^3,\omega^3)=g^{(2)}(1,2)g^{(2)}(1,3)g^{(2)}(2,3)\,\delta g^{(3)}(\mathbf{r}^3,\omega^3), \tag{1}$$

where $g^{(3)}$ is the three body correlation function and (1,2), for example, denotes the positions and orientations of molecules 1 and 2. The advantage of the latter, hierarchical, description is that the importance of each function is expected to decrease rapidly with N, as the difficulty of calculating it increases. Much of the information on the structure of a molecular fluid resides in the pair correlation function $g^{(2)}$. The triplet function $\delta g^{(3)}$ is also expected to be significant. It is generally presumed that the $\delta g^{(N)}$ functions for $N\geqslant 4$ rapidly approach unity as N increases.[10]

In atomic fluids with spherically symmetric interactions the pair correlation function can be obtained by standard integral equation theories.[9] Recently integral equation methods have been used for the calculation of the triplet correlation function as well.[11] In molecular fluids the PCF is a function of both the distance and the relative orientation of the molecules. Although the standard integral equations can be formally extended to include orientational degrees of freedom, solution of these equations is very laborious and necessitates the use of spherical harmonic expansions.[8] As an alternative, integral equations have been developed for the calculation of site–site correlation functions.[12,13] Several such equations have been applied to liquid water[14–16] with considerable success. However, site–site correlation functions are integrals over the molecular PCF and thus contain only part of the information in the full molecular PCF. The construction of the full PCF from site–site correlation functions is rigorously impossible because there are many PCFs consistent with one set of site–site correlation functions.[8]

Significant insights into the structure of liquid water have been obtained from computer simulations of realistic water models (e.g., Refs. 17–22). The simulations confirmed the basic picture of water as a continuous random network.[23,24] The structural information commonly reported from computer simulations of water is the atom–atom correlation functions. One reason for this is that these are the correlation functions obtained experimentally by x-ray and neutron diffraction techniques.[25,26] The second and more restrictive reason is the complexity of the molecular PCF. The PCF of water is a function of six variables: the distance between the oxygen atoms and five angles describing the relative orientation of the two water molecules. A function of six variables cannot be obtained directly from available computer simulations because the amount of sampling required to calculate a function grows exponentially with its dimensionality. With the currently available computer power, we cannot obtain functions of dimensionality higher than about 3 with a reasonable spacing between grid points. In simple atomic fluids the most complex function calculated by simulation is the triplet correlation function.[27,28] In the case of water, site–site triplet correlation functions have been recently obtained by computer simulation.[29]

Most of the work on orientational correlations in the past has focused on the Kirkwood g factor (the average of the cosine of the angle between the water dipoles) because it is related to the dielectric constant.[30–33] However, the g factor is not a *bona fide* measure of orientational correlations; i.e., its value does not reflect the extent to which molecular orientations are correlated (see below). Recently, Svishchev and Kusalik have used simulations to calculate the anisotropic distribution of the oxygen atom of one water molecule around a central water molecule and obtained insights into the nontetrahedral coordination in liquid water.[34,35] This provides useful information, but it involves an average over the orientations of the second molecule and, therefore, is still not the full PCF. The importance of the full PCF has been recently emphasized by Soper, who developed a method for the calculation of the smoothest possible PCF that would be consistent with experimentally (or theoretically) determined atom–atom correlation functions.[36] The PCF thus obtained has the minimum structure required by the information contained in the atom–atom correlation functions, but does not correspond to the true PCF.

In addition to providing insights into the structure of liquid water, the full PCF is important because it allows an approximate, first-principles calculation of the entropy based on an expression for the entropy of a fluid in terms of multiparticle correlation functions. This expression was derived by a number of authors.[37–41] The entropy expansion is briefly described in Sec. II. It has been used in practical calculations to estimate the entropy of simple fluids (reviewed in Ref. 42), such as the hard sphere fluid,[40,43–46] Lennard-Jones fluids,[28,45,47] liquid argon,[48] mixtures of hard spheres,[49] as well as molten salts,[41] liquid metals,[50] and model electrolytes.[51] For molecular fluids, calculation of the entropy requires the full PCF. No expression for an approximate evaluation of the entropy based on site–site correlation functions has been derived, though the entropy could be estimated from a PCF constructed by the method proposed by Soper.[36]

In this paper we attempt to develop approximations for the PCF of liquid water by taking advantage of the fact that the PCF can be calculated exactly in the low density limit (i.e., for two isolated interacting water molecules). We introduce and test two approaches for obtaining the liquid state PCF: The first is based on the factorization of the orientational distribution into functions of lower dimensionality. Various factorizations are examined and the best are selected based on their performance in the low-density limit. The second approach to the PCF of liquid water uses the low-density orientational distribution as a reference. This function is adjusted to give the correct orientationally averaged interaction energy in liquid water and to be consistent with the lower dimensionality orientational distributions obtained by simulation. These approaches are described in Sec. III.

With the above methods for estimation of the PCF, we calculated the two-particle contribution to the entropy at different temperatures. Contributions to the entropy from higher order terms in the correlation expansion are not calculated here, but their importance can be inferred by comparison of the two-particle result with the excess entropy of water obtained theoretically or experimentally. The variation of the two-particle entropy with temperature was used to obtain an estimate for the heat capacity. The effect of pressure on the orientational correlations and the entropy was also studied. Interestingly, it was found that an increase in pressure (density) leads to a decrease in orientational correlations and the magnitude of the orientational entropy. The results are presented in Sec. IV and a discussion of the present approach is given in Sec. V.

II. THEORY AND METHODS

The entropy of a fluid can be expressed as a sum of integrals over multiparticle correlation functions.[41,47] For a molecular fluid[52] this expression is

$$s = s^{\mathrm{id}} - \frac{1}{2} k \frac{\rho}{\Omega^2} \int [g^{(2)} \ln g^{(2)} - g^{(2)} + 1] d\mathbf{r}\, d\omega^2 - \frac{1}{3!} k \frac{\rho^2}{\Omega^3} \int [g^{(3)} \ln \delta g^{(3)} - g^{(3)} + 3g^{(2)} g^{(2)} - 3g^{(2)} + 1] d\mathbf{r}^2\, d\omega^3 - \cdots , \quad (2)$$

where, k is Boltzmann's constant, ρ is the number density of the fluid, and Ω the integral over the Euler angles of one molecule ($8\pi^2$ for nonlinear molecules). In Eq. (2) ω denotes the orientational variables of one molecule and $\mathbf{r}$ the relative position of two molecules. $g^{(2)}$ is a function of (r,ω^2), i.e., the relative position of the two molecules and their orientations. $g^{(3)}$ and $\delta g^{(3)}$ are a function of (r^2,ω^3), i.e., the relative position of two molecules from a third and the orientations of the three molecules. This expression can be applied in both the canonical and grand canonical ensembles.[47] The difference between the two ensembles is in the asymptotic behavior of the correlation functions. They go to unity in the grand canonical ensemble and to $1+O(1/N)$ in the canonical ensemble. The first term, s^{id}, is the entropy of an ideal gas at the same temperature and density, which is an upper limit to the entropy. The value of the ideal gas contribution for liquid water at 300 K and 1 atmosphere pressure is 30.8 e.u. Of this 10.5 e.u. is rotational entropy and 20.3 e.u. is translational entropy.[2] The second term accounts for correlations between two particles, the third term for correlations among three particles and so on.

Equation (2) provides a physical interpretation of the entropy of a fluid. The more the particles are correlated in their positions and orientations, the lower the entropy will be. In the two particle term, the $(-g+1)$ component accounts for the excluded volume effect and the logarithmic component for the ''order'' that exists in the fluid. This can be seen by considering a ''structureless'' fluid with g equal to 1 everywhere except within the hard core ($r<$diameter of particles). This is the result for a hard sphere fluid in the low density limit. The $g \ln g$ term in this case is zero and the only contribution to the entropy comes from the $(-g+1)$ term. A correlation function that is highly structured such as that expected for water (i.e., with high and narrow peaks and low valleys), is indicative of a more ordered system and tends to give an excess entropy that is more negative than that of a system with a smoother correlation function. For example, the excess entropy of liquid water is about -14 e.u. (1 e.u.$=1$ cal/mol K) whereas the excess entropy of the Lennard-Jones fluid at similar density is about -7 e.u.[47]

In simple hard sphere and Lennard-Jones fluids it was found that the two particle term in the entropy expansion accounts for 85%–95% of the total excess entropy by comparison with experimental and theoretical estimates of the entropy.[42,45,47] The two particle term has not yet been calculated for pure molecular fluids, although it has been estimated for atomic solvation in water.[52,53] In the latter work, only solute-water orientational correlations were considered, which are much easier to obtain because for spherically symmetric solutes they are a function of only two angles.

To evaluate the two-particle term for liquid water we separate it into a translational and an orientational contribution. This means that the pair correlation function is written

$$g(r,\omega^2) = g^r(r) g(\omega^2|r), \quad (3)$$

where, for notational simplicity, we dropped the superscript (2) from the pair correlation function. The first factor is the radial distribution function (RDF) for some arbitrary site in the molecules (in the case of water we take that to be the oxygen atom); i.e.,

$$g^r(r) = \frac{1}{\Omega^2} \int g(r,\omega^2) d\omega^2 \quad (4)$$

and the second factor, $g(\omega^2|r)$, is the conditional distribution function for the relative orientation of the two molecules given that the distance is r. We refer to this function as the orientational distribution function (ODF). It is normalized such that

$$\frac{1}{\Omega^2} \int [g(\omega^2|r) d\omega^2 = 1. \quad (5)$$

By substituting Eq. (3) into Eq. (2) and using the normalization condition, Eq. (5), the two particle entropy can be divided into a translational and an orientational part

$$s^{(2)} = \mathbf{s}^{(2)}_{\mathrm{trans}} + \mathbf{s}^{(2)}_{\mathrm{or}}, \quad (6)$$

where, by definition

$$s^{(2)}_{\mathrm{trans}} = -\frac{1}{2} k\rho \int [g^r(r) \ln g^r(r) - g^r(r) + 1] d\mathbf{r} \quad (7)$$

and

$$s^{(2)}_{\mathrm{or}} = \rho \int g^r(r) S^{\mathrm{or}}(r) d\mathbf{r} \quad (8)$$

with

$$S^{\mathrm{or}}(r) = -\frac{1}{2} k \frac{1}{\Omega^2} \int g(\omega^2|r) \ln g(\omega^2|r) d\omega^2. \quad (9)$$

The above decomposition is exact, though so far it is purely formal. The translational contribution arises from restriction of the radial distance between molecules and the orientational contribution from the restriction of the relative orientation of the molecules in the liquid.

The translational excess entropy can be evaluated straightforwardly using the oxygen–oxygen correlation function obtained from either experiment or simulations. In this work we concentrate on the orientational contribution to the excess entropy for which the ODF in Eq. (9) is needed. We estimate the ODF by using the results of calculations of an isolated TIP4P dimer in the gas phase (low density limit) and

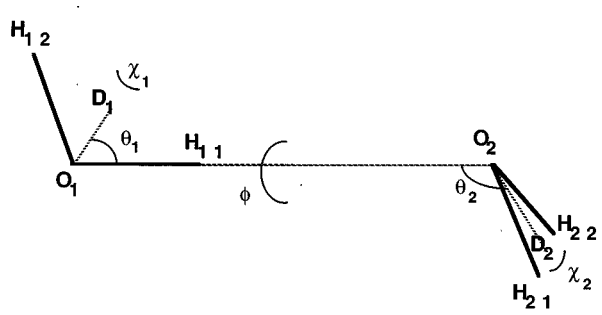

FIG. 1. The five angles defining the relative orientation between two water molecules. They are defined in terms of the following unit vectors: $\cos\theta_1 = \widehat{O_1D_1} \cdot \widehat{O_1O_2}$; $\cos\theta_2 = \widehat{O_2D_2} \cdot \widehat{O_2O_1}$; $\cos\phi = (\widehat{O_1O_2}\mathrm{X}\widehat{O_1D_1}) \cdot (\widehat{O_2D_2}\mathrm{X}\widehat{O_2O_1})$; $\cos\chi_1 = \widehat{H_{11}H_{12}} \cdot (\widehat{O_1O_2}\mathrm{X}\widehat{O_1D_1})$; $\cos\chi_2 = \widehat{H_{21}H_{22}} \cdot (\widehat{O_2D_2}\mathrm{X}\widehat{O_2O_1})$; H11 is taken to be the hydrogen of 1 closest to O2 and similarly for H21. The configuration shown corresponds to the global energy minimum for the TIP4P dimer, observed at $r=2.75$ Å and $\theta_1=52°$, $\theta_2=135°$, $\phi=180°$, $\chi_1=90°$, $\chi_2=0°$.

Monte Carlo simulations of liquid water. In the results section (Sec. III) we give both the translational and orientational contributions.

A. Gas phase calculations

The five angles that define the relative orientation of two water molecules are shown in Fig. 1. θ_1 and θ_2 are the angles between the dipole vector of each molecule and the intermolecular axis, ϕ (equal to the difference of the two Euler angles $\phi_1-\phi_2$) describes rotation around the intermolecular axis, and χ_1 and χ_2 describe the rotation of each water molecule around its dipole vector. The angles θ_1 and θ_2 vary from 0 to π and the other angles from 0 to 2π. The definition of the angles is given in the legend of Fig. 1.

The pair correlation function in the gas phase in the low density limit is[54]

$$g(r,\omega^2)=\exp[-\beta u(r,\omega^2)], \tag{10}$$

where $\beta=1/kT$ and $u(r,\omega^2)$ is the interaction energy. When we factor $g(r,\omega^2)$ according to Eq. (3) in the low density limit, the RDF is

$$g^r(r)=\frac{1}{\Omega^2}\int \exp[-\beta u(r,\omega^2)]d\omega^2 \tag{11}$$

and the ODF is

$$g(\omega^2|r)=\frac{\Omega^2\exp[-\beta u(r,\omega^2)]}{\int \exp[-\beta u(r,\omega^2)]d\omega^2}, \tag{12}$$

where

$$\int d\omega^2=\int \sin\theta_1\, d\theta_1 \sin\theta_2\, d\theta_2\, d\phi_1\, d\phi_2\, d\chi_1\, d\chi_2$$

$$=2\pi\int \sin\theta_1\, d\theta_1 \sin\theta_2\, d\theta_2\, d\phi\, d\chi_1\, d\chi_2.$$

To calculate $g(\omega^2|r)$ we need to perform the integration of the Boltzmann factor over all relative orientations. We do that by varying all five angles at 10° intervals for each distance r. [A 6° interval gives a value for the orientationally averaged interaction energy [see Eq. (14) below] differing in the fourth decimal point at $r=2.8$ Å]. In doing so we can take advantage of the symmetries in g: First, the two molecules are interchangeable, so we can integrate θ_1 from 0 to π and θ_2 from θ_1 to π. Second, the C_{2v} symmetry of the water molecule allows us to integrate χ_1 and χ_2 only from 0 to π. Finally, because $g(\phi,\chi_1,\chi_2)= g(2\pi-\phi,\pi-\chi_1, \pi-\chi_2)$, we can integrate ϕ only from 0 to 180.

To determine the interaction between two (rigid) water molecules we use the TIP4P model,[19] which is a refinement of the four-center water model proposed by Bernal and Fowler.[1] The TIP4P interaction potential has the form

$$u=4\epsilon\left[\left(\frac{\sigma}{r_{\mathrm{OO}}}\right)^{12}-\left(\frac{\sigma}{r_{\mathrm{OO}}}\right)^{6}\right]+\sum_{ij}\frac{q_iq_j}{\epsilon r_{ij}} \tag{13}$$

where r_{ij} are interatomic distances, q_i the partial charges, and ϵ is a dielectric constant ($\epsilon=1$). The Lennard-Jones parameters are $\sigma=3.153\,65$ Å and $\epsilon=0.155$ kcal/mol. The partial charges are $+0.52$ for the hydrogen atoms and -1.04 for the center of negative charge located at a distance of 0.15 Å from the oxygen atom along the HOH angle bisector; the OH bond length is 0.9572 Å and the HOH angle is 104.52°. In this equation the energy is expressed in terms of atom–atom distances. Consequently, to calculate the integral of the Boltzmann factor we need to transform from the five angles to a Cartesian coordinate system, which is computationally the most expensive task.

The orientationally averaged interaction energy as a function of r in the low density limit is calculated from the equation

$$U^{\mathrm{or}}(r)=\frac{1}{\Omega^2}\int g(\omega^2|r)u(r,\omega^2)d\omega^2$$

$$=\frac{\int u(r,\omega^2)\exp[-\beta u(r,\omega^2)]d\omega^2}{\int \exp[-\beta u(r,\omega^2)]d\omega^2}. \tag{14}$$

B. Monte Carlo simulations

Monte Carlo simulations of pure water were performed with the program BOSS, version 2.8[55] at temperatures from 5 to 65 °C and constant pressure of 1 atm. Simulations were also performed at 25 °C and 10000 atm. 216 TIP4P water molecules in a cubic box were simulated starting from an equilibrated box of TIP4P molecules. A spherical cutoff of 8.5 Å was used, quadratically switched off from 8 Å. Equilibration lasted at least 1 million configurations and the distribution functions were calculated over 10 million configurations. The results from four segments of 2.5 million configurations each were used to estimate the statistical error. Uncertainties due to the approximations for the ODF are expected to be significantly larger. However, they are difficult to estimate. The program was modified to obtain the $1d$ and $2d$ marginal orientational distribution functions. The marginal distribution functions[56] are defined as the probabil-

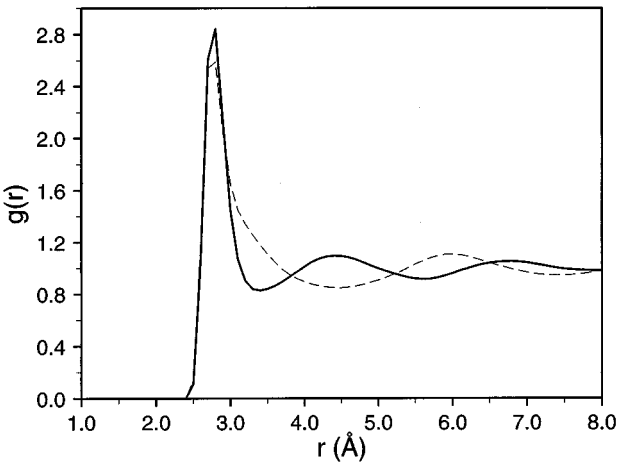

FIG. 2. Oxygen–oxygen radial distribution function at 25 °C, 1 atm (solid line) and 25 °C, 10000 atm (dashed line).

ity distributions of one angle or the joint probability distributions of two angles regardless of the value of the remaining angles; i.e.,

$$g(\omega_i|r)=\frac{\int g(\omega^2|r)d\omega_{j\neq i}}{\int d\omega_{j\neq i}} \tag{15}$$

and

$$g(\omega_i,\omega_j|r)=\frac{\int g(\omega^2|r)d\omega_{k\neq i,j}}{\int d\omega_{k\neq i,j}}. \tag{16}$$

They can be thought of as projections of the full ODF onto one or two dimensions. Here, ω_i or ω_j denote any one of the angles describing the relative orientation of two molecules $(i\neq j)$, and $d\omega_{k\neq i,j}$ represents the integration over all angles other than ω_i or ω_j. At each step, for every pair of molecules at a mutual distance of 5.6 Å (the second minimum of the radial distribution function) or less, the angles $\theta1,\theta2,\phi,\chi1,\chi2$ (see Fig. 1) were calculated and the distributions $g(\omega_i|r)$ and $g(\omega_i,\omega_j|r)$ for all angles ω_i,ω_j, $(i,j=1,5$ and $i\neq j)$ were accumulated at 10° intervals. These orientational distributions were calculated for three ranges of r (see Fig. 2): the first subshell of the first neighbor shell ($r\leqslant2.8$ Å), the second subshell of the first neighbor shell ($2.8<r\leqslant3.4$ Å), and the second neighbor shell ($3.4<r\leqslant5.6$ Å). This choice allows a reliable calculation of the orientational distributions in a reasonable amount of computer time (10 million configurations). At 25 °C the orientational distributions were also calculated at finer distance resolution, over regions of 0.2 Å. For these calculations, sampling of 70 million configurations was necessary.

Similar simulations (1 million configurations each) were used to calculate the orientationally averaged interaction energy between two water molecules as a function of distance

$$U^{\mathrm{or}}(r)=\frac{1}{\Omega^2}\int g(\omega^2|r)u(r,\omega^2)d\omega^2. \tag{17}$$

This quantity is straightforward to obtain from the simulation since it is the average interaction energy between two water molecules at a given distance regardless of their orientation (i.e., the orientational average is done implicitly by the simulation). In terms of the orientationally averaged interaction energy, the excess molar energy of the fluid can be written

$$e=\frac{1}{2}\frac{\rho}{\Omega^2}\int g(r,\omega^2)u(r,\omega^2)d\omega^2\ d\mathbf{r}$$

$$=\frac{1}{2}\rho\int g^r(r)U^{\mathrm{or}}(r)d\mathbf{r}. \tag{18}$$

The molar enthalpy can be obtained by adding the kinetic energy contribution and the PV term, the latter being negligible for a liquid at ambient pressure.

It has been reported that the truncation of the long range interactions in simulations of water significantly affects orientational correlations at short range[57–59] but the cutoffs which proved inadequate in these studies were very short (less or equal to 6 Å). To check the effect of the spherical cutoff used, the orientationally averaged pair interaction was also obtained from a simulation of 512 molecules with a cutoff of 11.5 Å. The difference in the two calculations was comparable to the statistical uncertainty ($\leqslant$0.2 kcal/mol at all distances).

The proposed approximations to the ODF of liquid water can be checked for consistency with the site–site distribution functions obtained directly from the simulation. The site–site distribution functions result from integration of the molecular PCF[9]

$$g_{\alpha\beta}(\mathbf{r})=\frac{1}{\Omega^2}\int g(\mathbf{R}_{12},\omega^2)\,\delta(\mathbf{R}_{\alpha\beta}(\mathbf{R}_{12},\omega^2)-\mathbf{r})d\omega^2\ d\mathbf{R}_{12}, \tag{19}$$

where α,β are sites on the molecule, $\mathbf{R}_{12}$ is the vector between two molecular centers, and $\mathbf{R}_{\alpha\beta}$ is the vector between two sites α and β. In terms of scalar distances

$$4\pi r^2 g_{\alpha\beta}(r)=\frac{1}{\Omega^2}\int 4\pi R_{12}^2 g(R_{12},\omega^2)$$

$$\times\,\delta(R_{\alpha\beta}(R_{12},\omega^2)-r)d\omega^2\ dR_{12}, \tag{20}$$

where we have used for any X that

$$\int X\,\delta(\mathbf{R}_{\alpha\beta}-\mathbf{r})d\mathbf{R}_{12}=\int X\,\delta(R_{\alpha\beta}-r)dR_{12}/4\pi r^2. \tag{21}$$

The OH and HH distribution functions are obtained by performing the above integration numerically using the two proposed approximations for $g(R_{12},\omega^2)$ and compared to those obtained directly by simulation.

III. APPROXIMATIONS FOR THE PAIR CORRELATION FUNCTION

The basic assumption of the present approximations for the PCF is that the orientational distribution function in liquid water and its low-density gas-phase counterpart have similar structure; i.e., they are both expected to exhibit maxima at orientations permitting hydrogen bonding and minima at repulsive configurations. In the liquid the orientational distribution should be ''smoother'' because of the

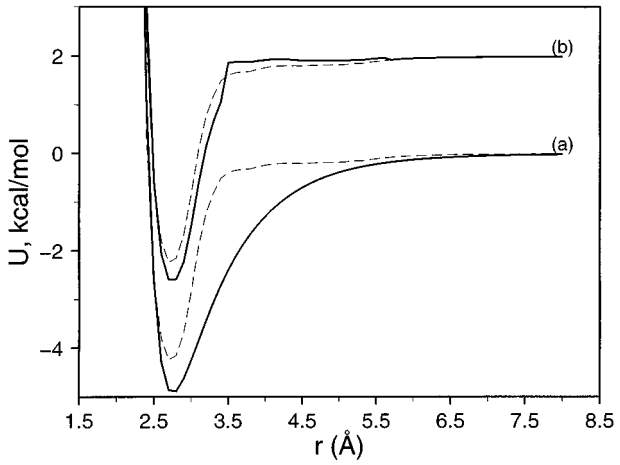

FIG. 3. (a) Orientationally averaged interaction energy in the gas (solid line) and in the liquid (dashed line). (b) Orientationally averaged interaction in the AGP approximation (solid line) compared to the exact one from the simulation (dashed line). Curves (b) have been shifted by 2 kcal/mol along the y axis for clarity. All results at 25 °C, 1 atm, unless noted otherwise.

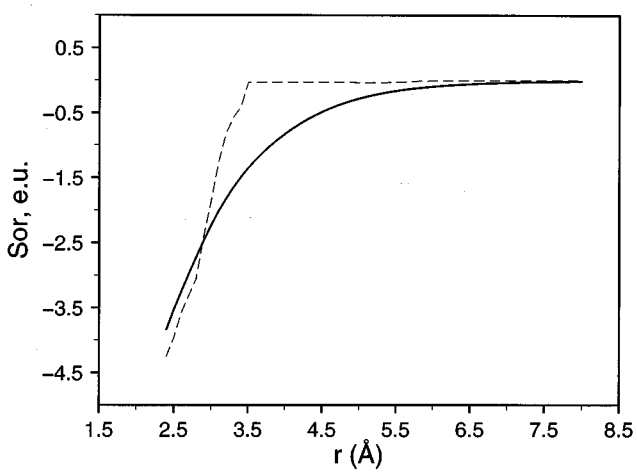

FIG. 4. Orientational entropy integrand in the gas (solid line) and in the AGP approximation for the liquid (dashed line).

presence of other water molecules in the surroundings. The low density gas-phase ODF was calculated as described above for the TIP4P interaction potential. The TIP4P model is an effective pairwise potential meant to represent water in the condensed phase and implicitly includes the effects of polarization and many-body forces. Thus, it is more appropriate for our purposes than the actual gas-phase potential.

We first study the TIP4P dimer and calculate its orientationally averaged energy and orientational entropy as a function of distance. The $1d$ and $2d$ orientational marginal distribution functions (see Sec. II) are calculated at a number of distances and compared to those calculated in the liquid by simulation. This work is presented in Sec. III A.

Factorization of the ODF into products of $2d$ marginals is considered in Sec. III B. Several factorizations are empirically tested by applying them to the gas phase ODF. It is assumed that factorizations which work well in the gas phase will work in the liquid.

A different approach is explored in Sec. III C. The gas-phase ODF is first uniformly smoothed in order to reproduce the calculated orientationally averaged interaction in the liquid and then adjusted to bring it in agreement with the calculated liquid-phase marginals.

A. The low-density limit and comparison with the liquid

The calculated orientationally averaged energy in the gas is shown in Fig. 3(a) and compared to the orientationally averaged energy in the liquid obtained by simulation. Both refer to a temperature of 25 °C, but similar results were obtained at all temperatures. Overall, the interaction in the gas is stronger and falls off more slowly with distance, as expected. The largest difference is observed between 2.7 and 4.5 Å. This includes the peak of the RDF, the first minimum and part of the second maximum (see Fig. 2). Overall, the ODF is more ''structured'' in the gas phase. This results from the fact that in the liquid water molecules can experience favorable interactions at many more orientations than in the gas phase, where they have only one partner. The orientational entropy integrand, $S^{\mathrm{or}}(r)$, in the gas is given by the solid line in Fig. 4. Its magnitude as a function of distance is seen to decrease asymptotically to zero.

In 1972 Ben-Naim and Stillinger[60] considered the following approximation to the PCF of water:

$$g(r,\omega^2)=y(r)\exp[-\beta u(r,\omega^2)], \tag{22}$$

where

$$y(r)=g^r(r)/\lim_{\rho\to 0} g^r(r)$$

and $g^r(r)$ is the experimentally determined liquid phase RDF. This approximation is equivalent to using the liquid RDF and assuming, in our notation, that the ODF of the liquid is identical to the low-density gas-phase ODF. With this approximation, they calculated the Kirkwood g_k factor[61]

$$g_k=1+\frac{\rho}{\Omega^2}\int \cos\,\theta g(r,\omega^2)d\mathbf{r}\,d\omega^2$$

$$=1+\rho\int\langle\cos\,\theta\rangle_r g^r(r)d\mathbf{r}, \tag{23}$$

where θ is the angle between the dipole vectors of two water molecules. [This angle does not correspond to any of the five angles defined here but it is a function of θ_1, θ_2, and ϕ.] This factor was found to be smaller than the value expected from the experimental dielectric constant of water (1.94 compared to the experimental value of 2.9). They took this to mean that orientational correlations in the liquid are actually stronger than in the gas, presumably due to the tetrahedral packing in the condensed phase. This conclusion seems to contradict the statement made above based on the orientationally averaged interaction. The reason is that the Kirkwood factor g_k is a measure of correlations between the water dipoles, i.e., it is a rather restricted measure of orientational correlation. The orientational distribution may seem more or less structured de-

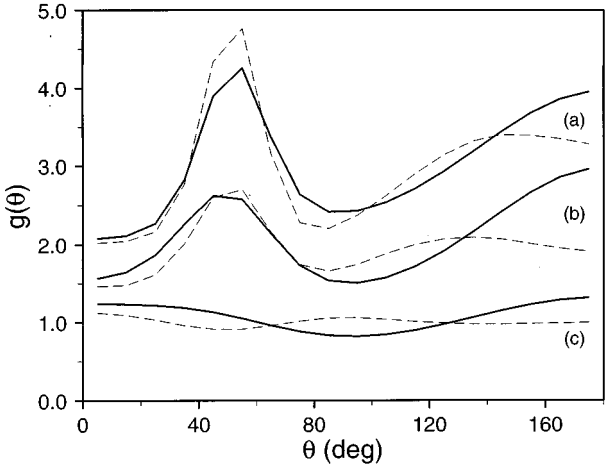

FIG. 5. The distribution function $g(\theta)$ in the gas (solid line) and in the liquid (dashed line). (a) $r=2.8$ Å in the gas, $r\leqslant 2.8$ Å in the liquid (b) $r=3.2$ Å in the gas, $2.8\leqslant r\leqslant 3.4$ Å in the liquid (c) $r=4.5$ Å in the gas, $3.4\leqslant r\leqslant 5.6$ Å in the liquid. Curves (a) and (b) have been shifted along the y axis by 2 and 1, respectively.

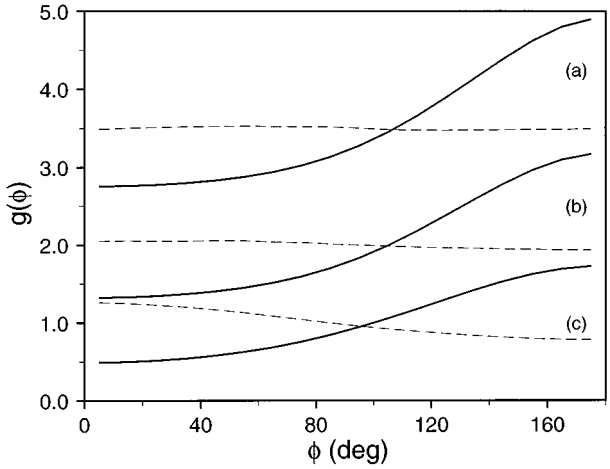

FIG. 7. The distribution function $g(\phi)$ in the gas (solid line) and in the liquid (dashed line). (a), (b), and (c) as in Fig. 5. Curves (a) and (b) have been shifted along the y axis by 2.5 and 1, respectively.

pending on which features or which slice of it is being examined. The comparison of the marginal distributions below suggests a reason why the gas phase ODF underestimates g_k despite the fact that it is more structured in an overall sense.

Knowing the ODF in the gas phase, we can calculate the $1d$ and $2d$ marginals using Eqs. (15) and (16). These marginals were calculated at three distances corresponding to the three regions over which the same marginals were calculated in the liquid by simulation: 2.8, 3.2, and 4.5 Å. The $1d$ marginals are shown in Figs. 5, 6, and 7 and compared to the corresponding distributions from the liquid simulations. All figures in this section refer to a temperature of 25 °C.

The θ (θ_1 or θ_2) distribution in the gas phase at 2.8 Å [Fig. 5(a)] shows two maxima: a narrow one at about 50°, corresponding to the tetrahedral hydrogen bond donor configuration, and a broader maximum at 180°, corresponding to the hydrogen bond acceptor configuration. Thus, although the global minimum energy configuration (Fig. 1) occurs for $\theta_1=52°$, $\theta_2=135°$, the most probable value of θ_2 turns out to be closer to 180° when the thermal average over all configurations is taken. In the liquid, the hydrogen bond donor peak is slightly enhanced and the hydrogen bond acceptor maximum shifts to about 140°, which corresponds to almost tetrahedral coordination (perfect tetrahedral would be 125°). This latter shift reflects the fact that the tetrahedrality on the hydrogen bond acceptor side is induced by packing effects in the liquid and it is not intrinsic to the TIP4P potential (see also, Ref. 34). The ST2 model, which has explicit lone pair sites, exhibits tetrahedral preferences in the isolated dimer.[62]

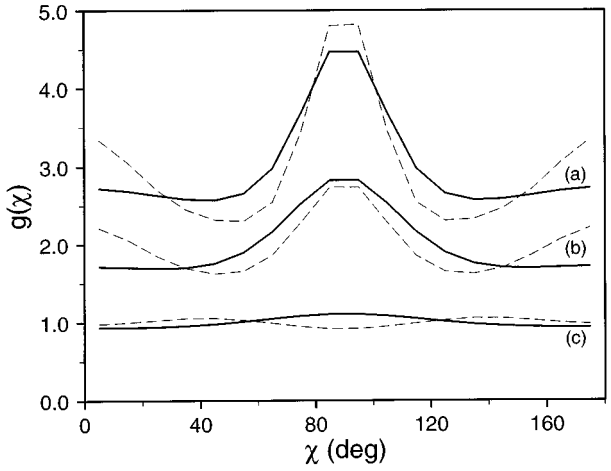

FIG. 6. The distribution function $g(\chi)$ in the gas (solid line) and in the liquid (dashed line). (a), (b), and (c) as in Fig. 5. Curves (a) and (b) have been shifted along the y axis by 2 and 1, respectively.

The χ distribution at 2.8 Å [Fig. 6(a)] is also very similar in the gas and in the liquid but it is more structured in the liquid. The reason for this is the tetrahedrality at the hydrogen acceptor configuration induced by the liquid structure. The values 0° (180°) and 90° for χ are strongly preferred when θ_1 and θ_2 have their tetrahedral values (see Fig. 1). Thus increase in the probability of the tetrahedral θ values, [Fig. 5(a)] leads to an increase in the probability of 0° and 90° for χ.

The most dramatic qualitative difference between gas and liquid is seen in the ϕ distribution [Fig. 7(a)]. In the gas there is clear preference for antiparallel configurations ($\phi=180°$). In the liquid this preference is eliminated and the distribution is essentially flat. This is due to the existence of other water molecules around the central pair which obviate any necessity for the antiparallel arrangement. This change in the ϕ distribution is consistent with the observation of Ben-Naim and Stillinger[60] mentioned above that the g_k factor from the gas phase ODF is lower than the experimental value, since a decrease in antiparallel dipole configurations leads to an increase in the value of g_k. [This can be verified by evaluating the integral in Eq. (23) using the gas-phase ODF and the approximations to the liquid phase ODF presented below.] This is an example of how a *decrease* in correlations leads to an *increase* in g_k, which shows that g_k

is not a reliable measure of the extent of orientational correlations in liquid water.

Figures 5(b), 6(b), and 7(b) show the $1d$ marginals in the gas at $r=3.2$ Å and in the liquid between 2.8 and 3.4 Å. They are similar to those in the first subshell, only somewhat flatter. Figures 5(c), 6(c), and 7(c) show the $1d$ marginals in gas at 4.5 Å and in the liquid in the second neighbor shell (3.4 to 5.6 Å). The distributions are almost flat in this region in the liquid except for a slight reversal of preferences in θ,χ between gas phase and liquid. This reversal is probably due to the fact that the correlation between two water molecules in that range of distances is ''direct'' in the gas phase whereas it is ''indirect'' (through hydrogen bonding to an intervening water molecule) in the liquid. In the ϕ distribution there is a preference for small values of ϕ (parallel configurations) in the liquid.

For the $2d$ marginals, we show only the results in the first subshell of the first neighbor shell. The distributions in the second subshell are similar to those in the first subshell, only less pronounced. In the second neighbor shell the orientational correlations are very weak. The θ_1,θ_2 distribution in the first subshell in the liquid is shown in Fig. 8(a). The distribution is symmetric around the diagonal due to symmetry with respect to particle interchange. The maximum of the distribution is at about (50°,150°) corresponding to one molecule acting as a hydrogen-bond donor and the other as an acceptor. The distribution in the gas (not shown) is very similar, only the peaks are somewhat higher (the value is 11.74 vs 7.88 in the liquid).

The (θ_1,χ_1) distribution is shown in Fig. 8(b). The main maximum is at $\chi=90°,\theta=55°$ ($g=15.5$), which corresponds to the molecule acting as a hydrogen-bond donor. There is a very weak secondary maximum at $\theta=125°,\chi=0°$ ($g=3.14$), which corresponds to the molecule acting as an acceptor in a tetrahedral arrangement. In the gas, again, the distribution is very similar (not shown), except for the lack of tetrahedral preference for the acceptor configuration. Figure 8(b) is in good qualitative agreement with Fig. 5 of Ref. 34 (the angle ϕ in that work is equivalent to our $\chi_1-90°$). Quantitative differences are probably due to the difference in the water model used in the two studies (SPC/E vs TIP4P).

The θ_1,χ_2 distribution is shown in Fig. 8(c). The maxima are at $\theta=55°,\chi_2=0°$ (donor) and $\theta=150°,\chi=90°$ (acceptor). The two maxima have approximately equal height ($g=7.60$, 7.69). The χ_1,χ_2 distribution is shown in Fig. 8(d). Maxima occur at $\chi_1=90°,\chi_2=180°$ or vice versa. Again, one corresponds to a donor and the other to an acceptor configuration.

The (θ,ϕ) and (ϕ,χ) distributions are shown in Fig. 9. In the liquid, both of these $2d$ marginals are essentially parallel lines, i.e., $g(\phi,\alpha)=\text{const}\, g(\alpha)$, where α is χ or θ. In the gas these marginals look very different [Figs. 9(b) and 9(d)] because there is preference for antiparallel ϕ values (see Fig. 7). However, even in the gas, the coupling between ϕ and the other variables is relatively weak, i.e., the (θ,ϕ) and (ϕ,χ) marginals are almost a superposition of the corresponding $1d$ marginals.

In summary, the major differences between the distributions in the gas and in the liquid for nearest neighbors are the flatness with respect to ϕ and the small enhancement of tetrahedrality at the donor configuration in the latter. Other than that, the distributions are very similar. The flatness of the orientational distribution with respect to ϕ is very convenient because it reduces by one the number of degrees of freedom that need to be considered; i.e., $g(\theta_1,\theta_2,\phi,\chi_1,\chi_2|r)\approx\text{const}\; g(\theta_1,\theta_2,\chi_1,\chi_2|r)$. Of course, flatness of the $1d$ and $2d$ marginals with respect to ϕ does not prove that the higher dimensionality marginals are flat with respect to ϕ as well. However, it is a reasonable assumption.

The calculations of the above marginals as a function of r at a resolution of 0.2 Å showed that the decay of the orientational correlations with distance is smooth. As an example, the θ marginal is shown in Fig. 10 up to $r=3.7$ Å. The smooth decay of the correlations suggests that taking averages over ranges of r is appropriate; i.e., it does not introduce errors because of the slow variation in the orientational preferences as a function of distance. The situation is, however, more complex for higher dimensionality distribution functions, where inversion of the positions of the maxima and minima with distance have been observed.[34]

B. Factorizations of the orientational distribution

To find factorization schemes for use in estimating the ODF of the liquid, we employ the gas-phase results as a test case. The factorizations are applied to estimate the gas-phase ODF from the gas-phase $1d$ and $2d$ marginals and the results for U^{or} and S^{or} are compared with the exact results. In devising factorization schemes for the ODF in terms of the marginal distribution functions we bear in mind the following desirable properties for the approximate expressions: (a) they must satisfy the symmetries of $g(\omega^2|r)$, (b) they must give good U^{or} and S^{or} when applied to the low-density limit, and (c) they must be self-consistent, i.e., the marginals calculated from the approximate ODFs must be equal to the original marginals used as input.

1. Site superposition approximation

One proposed factorization scheme for the molecular pair correlation function is the site superposition approximation (SSA)[63] given by the equation

$$g(\omega^2|r)=\frac{\Pi_{\alpha\beta}g_{\alpha\beta}}{\langle\Pi_{\alpha\beta}g_{\alpha\beta}\rangle}, \tag{24}$$

where the denominator denotes an unweighted average over orientations

$$\left\langle\prod_{\alpha\beta}g_{\alpha\beta}\right\rangle=\frac{1}{\Omega^2}\int\prod_{\alpha\beta}g_{\alpha\beta}\,d\omega^2 \tag{25}$$

and $g_{\alpha\beta}$ are site–site (radial) correlation functions. This approximation was found to be qualitatively correct in diatomic hard sphere and Lennard-Jones fluid[64,65] but was unsatisfactory in atomic fluids with quadrupolar interactions.[66]

To apply the SSA to water we used

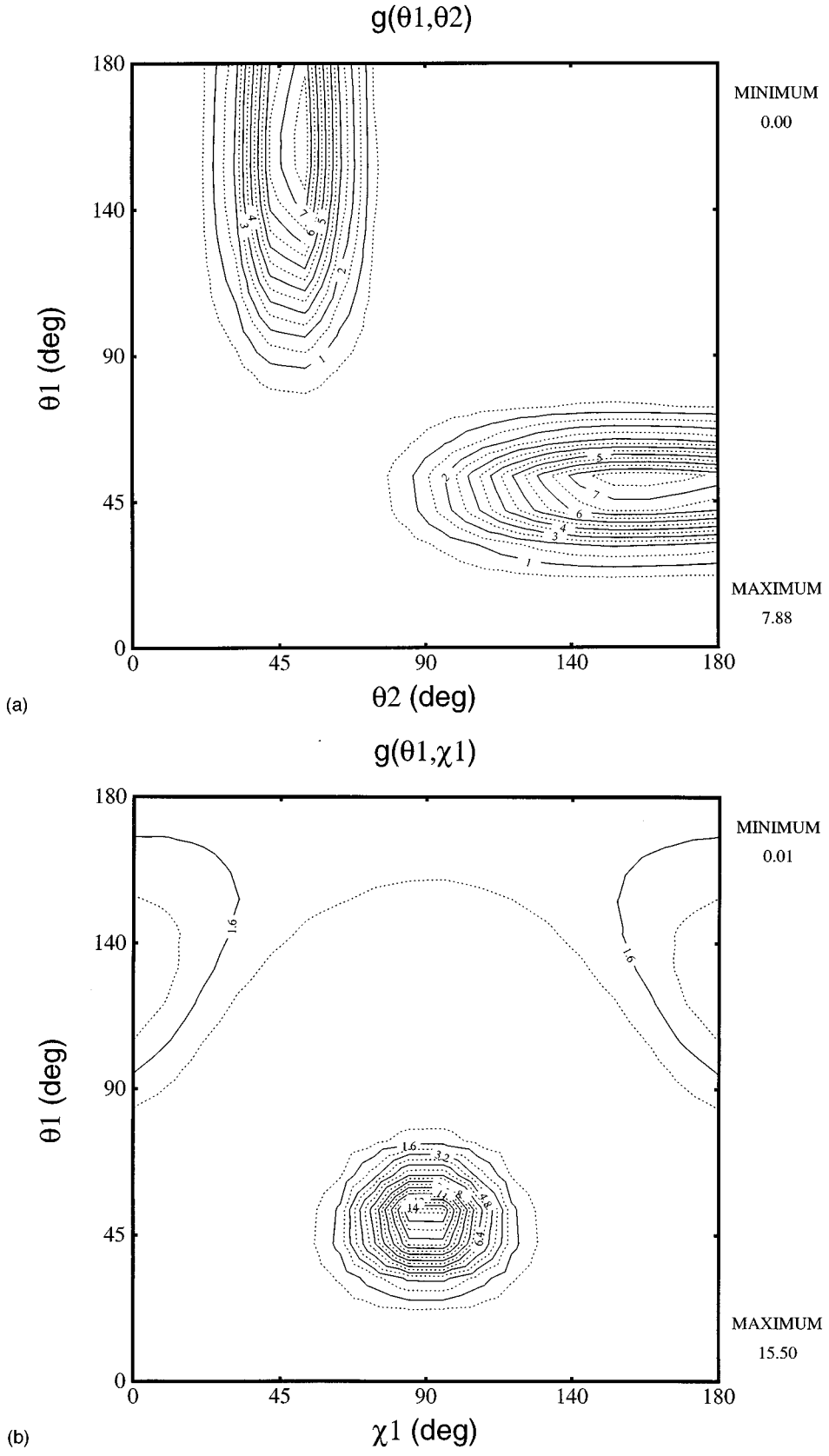

FIG. 8. Marginal distribution functions for the liquid in the first subshell ($r \leqslant 2.8$ Å) (a) $g(\theta_1,\theta_2)$, (b) $g(\theta_1,\chi_1)$, (c) $g(\theta_1,\chi_2)$, (d) $g(\chi_1,\chi_2)$.

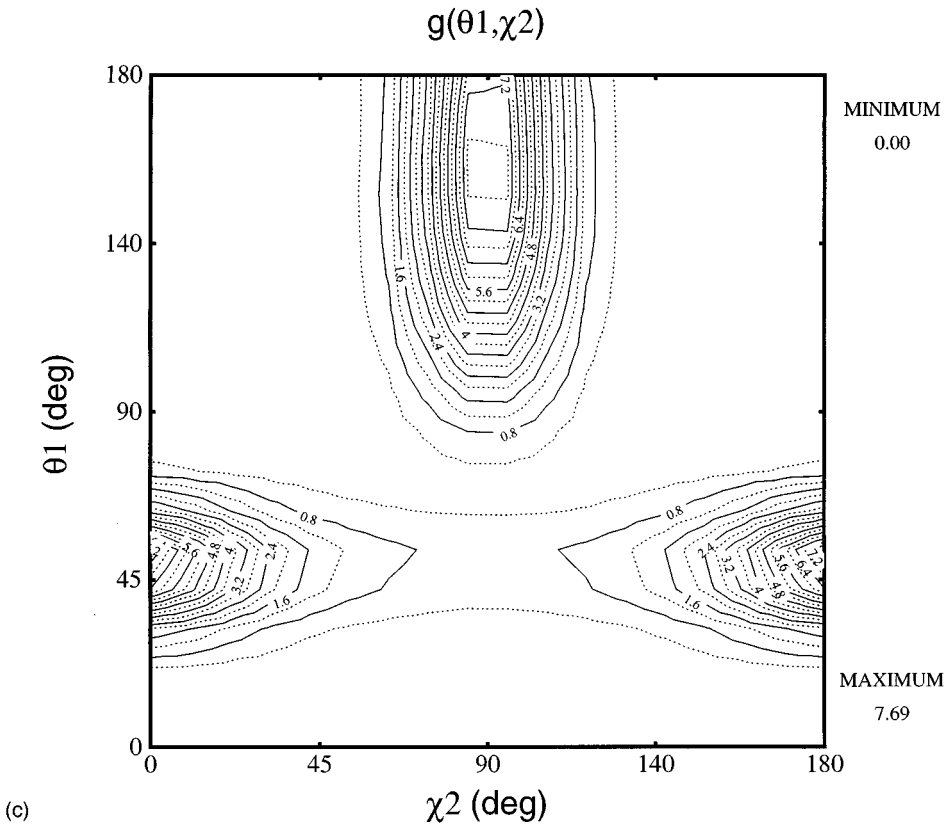

(c)

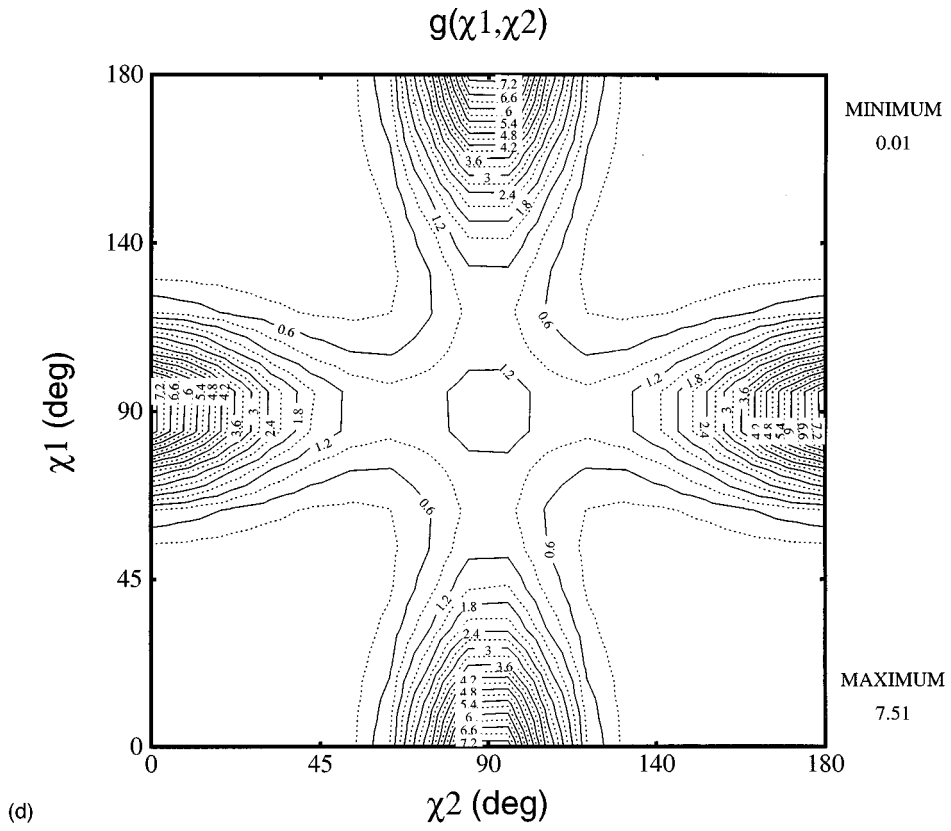

(d)

FIG. 8. (*Continued.*)

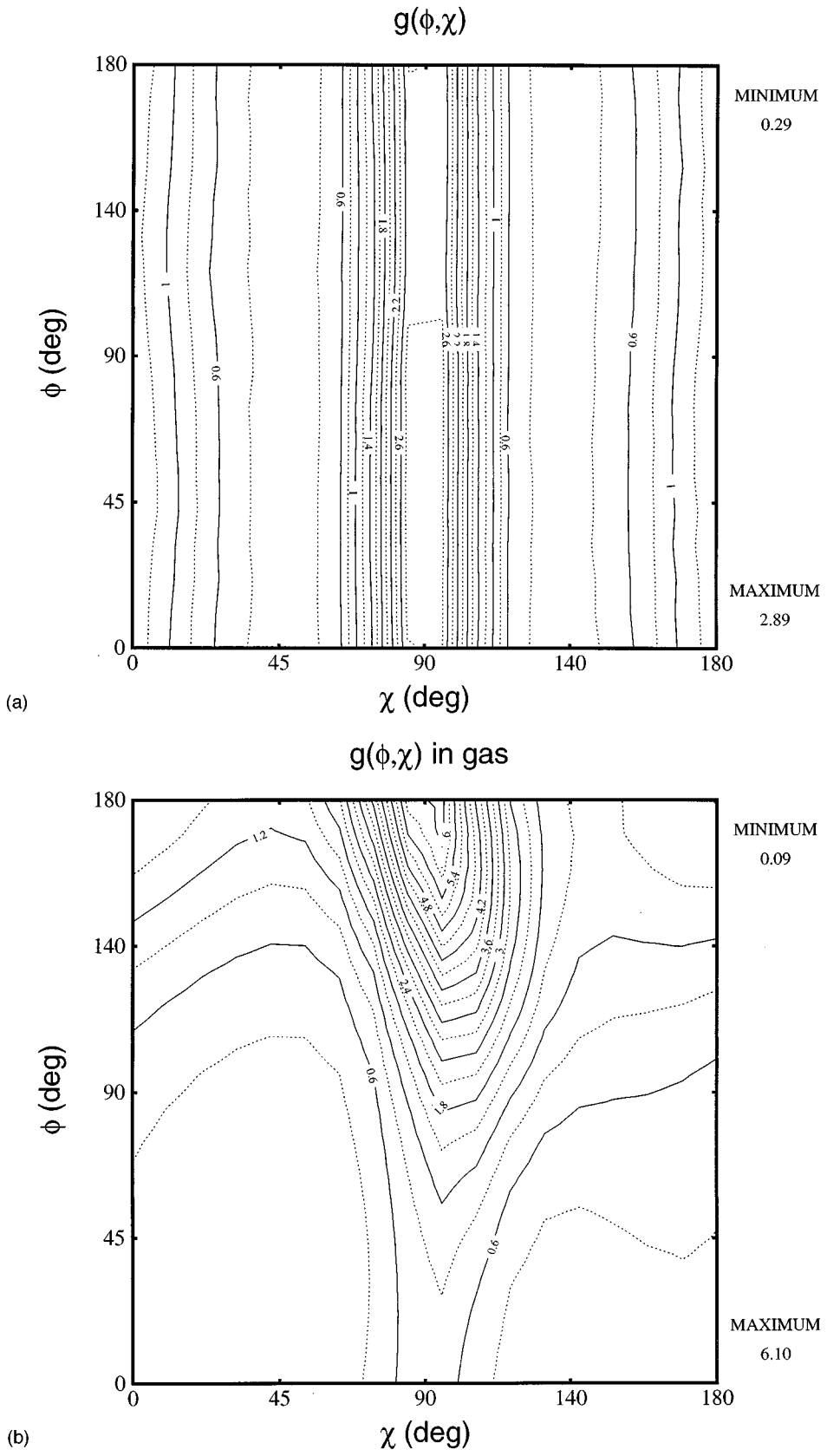

FIG. 9. Marginal distribution functions involving ϕ: (a) $g(\phi,\chi)$ for the liquid in the first subshell ($r \leqslant 2.8$ Å), (b) $g(\phi,\chi)$ in the gas at $r = 2.8$ Å, (c) $g(\theta,\phi)$ for the liquid in the first subshell ($r \leqslant 2.8$ Å), (d) $g(\theta,\phi)$ in the gas at $r = 2.8$ Å.

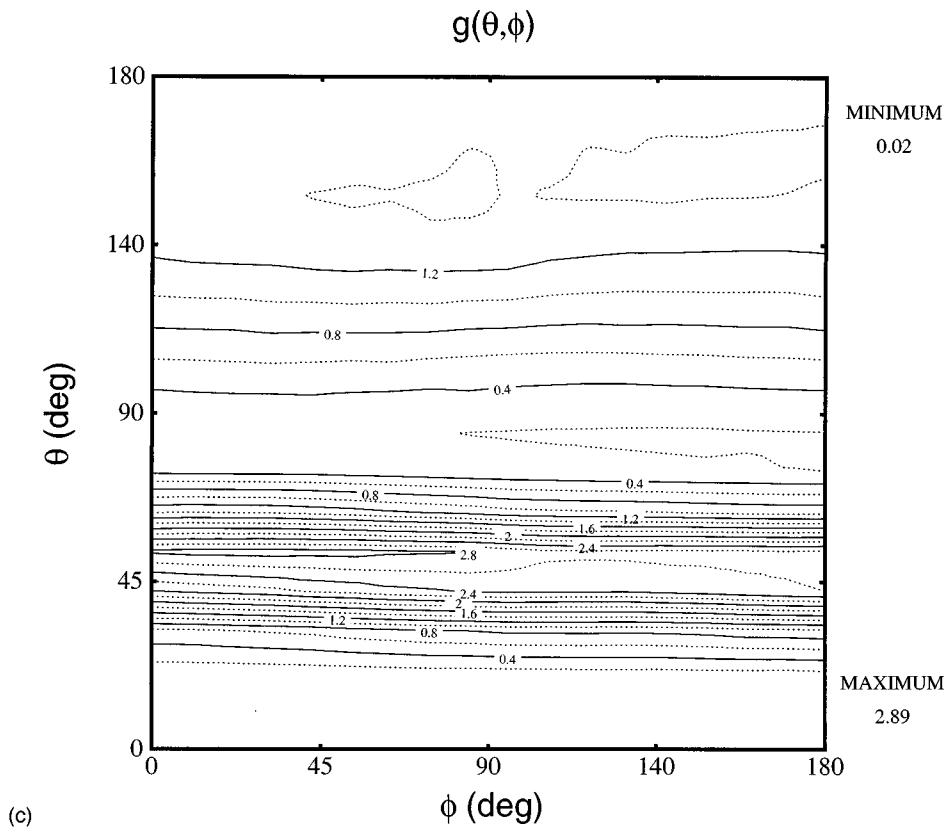

(c)

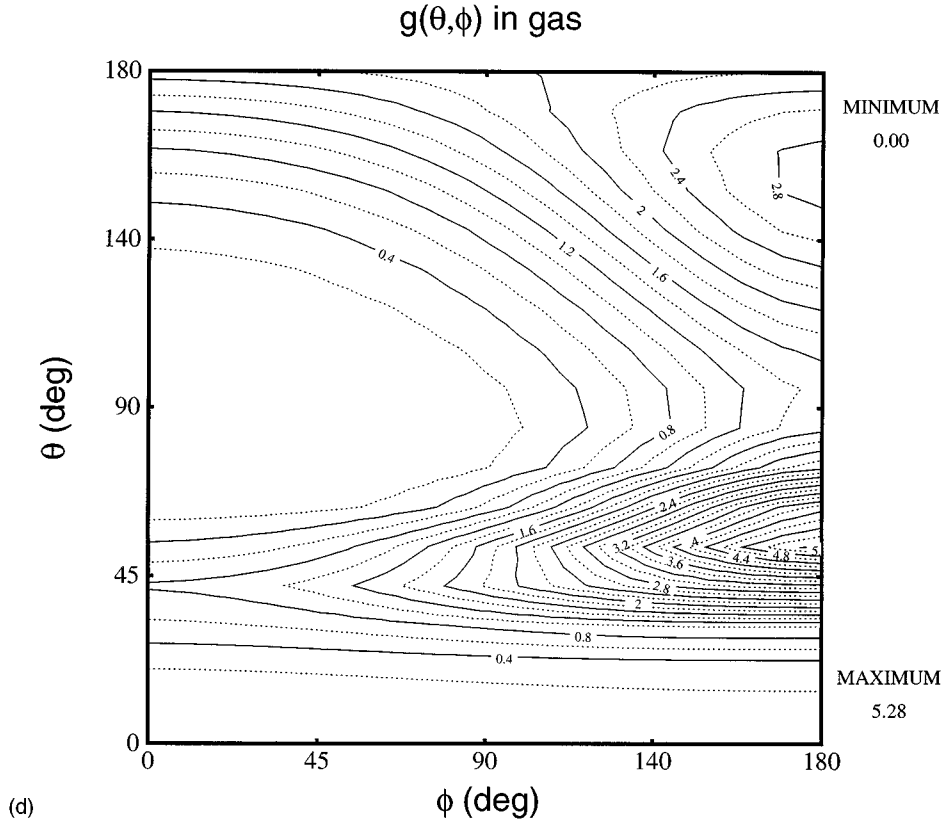

(d)

FIG. 9. (*Continued.*)

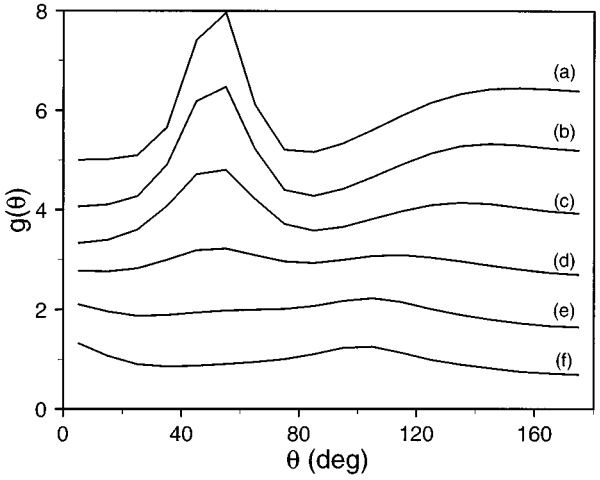

FIG. 10. The decay of $g(\theta)$ with distance in the liquid (a) $r=2.5-2.7$ Å, (b) $r=2.7-2.9$ Å, (c) $r=2.9-3.1$ Å, (d) $r=3.1-3.3$ Å, (e) $r=3.3-3.5$ Å, (f) $r=3.5-3.7$ Å. The curves have been shifted along the y axis for clarity.

$$\prod_{\alpha\beta} g_{\alpha\beta}=g_{O_1H_{21}}g_{O_1H_{22}}g_{O_2H_{11}}g_{O_2H_{12}}g_{H_{11}H_{21}}g_{H_{11}H_{22}} \times g_{H_{12}H_{21}}g_{H_{12}H_{22}}. \tag{26}$$

The site–site correlation functions for liquid TIP4P were obtained from the MC simulations and are essentially identical to those previously published.[19]

With this approximation we first calculated the orientationally averaged interaction in the liquid as a function of distance using Eq. (14) with Eqs. (24), (25), and (26). The results were poor. For example, U^{or} at 2.8 Å was calculated to be 2.73 kcal/mol instead of the correct value −4.15 kcal/mol. We also calculated $1d$ and $2d$ marginal orientational distribution functions at 2.8 Å and found them to be qualitatively incorrect. For example, Fig. 11 shows the joint probability of θ_1 and θ_2. It is very different from the correct distribution in Fig. 8(a).

2. Products of marginal distributions

Another simple factorization is to assume that the ODF is equal to the product of the $1d$ marginals

$$g(\omega^2|r)=\prod_i g(\omega_i|r). \tag{27}$$

Clearly, this would be exact if the angles were uncorrelated. This scheme cannot work because several $2d$ marginals have very different structure than the product of their $1d$ marginals at nearest neighbor distances (see Figs. 8–9). For example, $g(\theta_1)\ g(\theta_2)$ has a strong maximum at (55,55) but $g(\theta_1,\theta_2)$ does not.

An improved approximation is expected from products of the $2d$ marginals. In deciding the form of these products it is instructive to examine all $2d$ marginals and identify the ones which exhibit strong correlations, i.e., the ones that can-

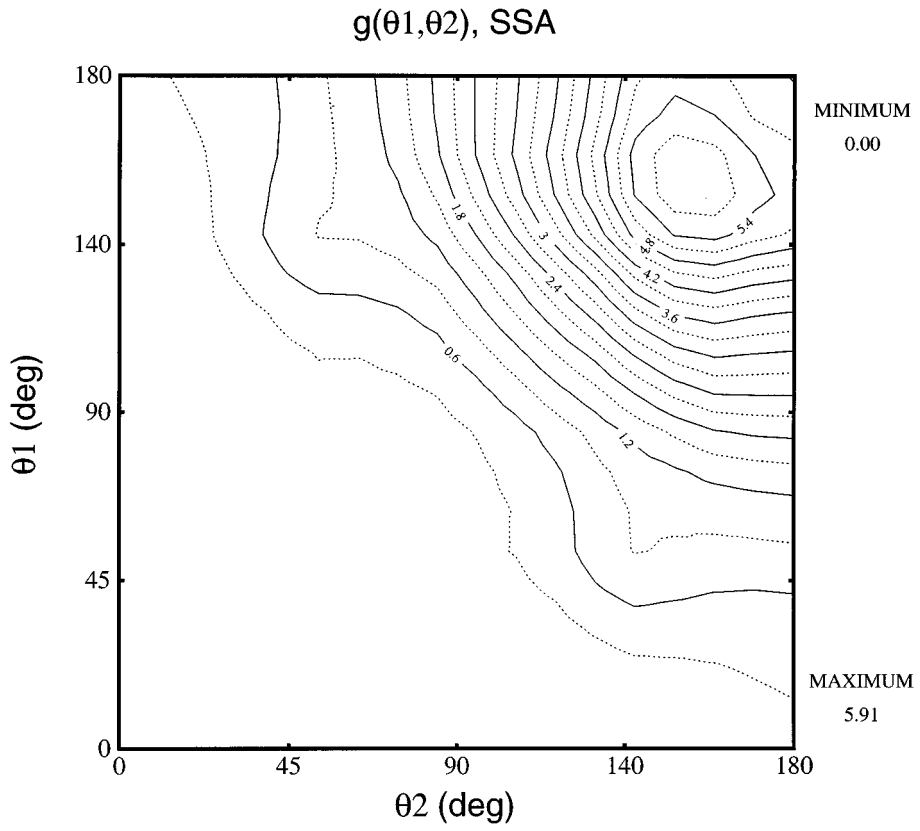

FIG. 11. $g(\theta_1,\theta_2)$ from the site superposition approximation at $r=2.8$ Å.

TABLE I. A few of the factorizations tested.

	$g(\theta_1,\theta_2,\phi,\chi_1,\chi_2)=$
$F1$	$g(\theta_1,\theta_2)\ g(\chi_1,\chi_2)\ g(\phi)$
$F2$	$g(\theta_1,\theta_2)\ g(\chi_1,\chi_2)\ g(\theta_1,\chi_2)\ g(\theta_2,\chi_1)\ g(\phi)$
$F3$	$g(\theta_1,\theta_2)\ g(\theta_1,\chi_1)\ g(\theta_2,\chi_2)\ g(\phi)/g(\theta_1)\ g(\theta_2)$
$F4$	$g(\chi_1,\chi_2)\ g(\theta_1,\chi_1)\ g(\theta_2,\chi_2)\ g(\phi)/g(\chi_1)\ g(\chi_2)$
$F5$	$g(\theta_1,\theta_2)\ g(\theta_1,\chi_2)\ g(\theta_2,\chi_1)\ g(\phi)/g(\theta_1)\ g(\theta_2)$
$F6$	$g(\chi_1,\chi_2)\ g(\theta_1,\chi_2)\ g(\theta_2,\chi_1)\ g(\phi)/g(\chi_1)\ g(\chi_2)$
$F7$	$g(\theta_1,\theta_2)\ g(\chi_1,\chi_2)\ g(\theta_1,\chi_2)\ g(\theta_2,\chi_1)\ g(\phi)/g(\theta_1)\ g(\theta_2)g(\chi_1)\ g(\chi_2)$
$F8$	$g(\theta_1,\theta_2)\ g(\theta_1,\phi)\ g(\theta_1,\chi_1)\ g(\theta_1,\chi_2)\ g(\theta_2,\phi)\ g(\theta_2,\chi_1)\ g(\theta_2,\chi_2)$ $g(\phi,\chi_1)\ g(\phi,\chi_2)\ g(\chi_1,\chi_2)/g(\theta_1)^3\ g(\theta_2)^3\ g(\phi)^3\ g(\chi_1)^3\ g(\chi_2)^3$

not be represented by the product of their $1d$ marginals. The functions $g(\theta_1,\theta_2)$, $g(\chi_1,\chi_2)$, and $g(\theta_1,\chi_2)$ belong to this category. In contrast, the marginals involving ϕ $[g(\phi,\chi),g(\phi,\theta)]$ and the marginal $g(\theta_1,\chi_1)$ are qualitatively similar to the product of their $1d$ marginals. This suggests that $g(\theta_1,\theta_2)$, $g(\chi_1,\chi_2)$ and $g(\theta_1,\chi_2)$ should be represented explicitly in the factorization, whereas ϕ could be represented by its $1d$ marginal (which in the liquid is flat, as shown above).

A number of such factorizations is shown in Table I. About 35 other factorizations were tested (products of four or five $2d$ marginals) but they are not reported since they were similar or inferior in performance to those in Table I. We can determine the quality of each factorization by applying it to the gas phase TIP4P dimer. Table II shows the results for the orientationally averaged energy, the orientational entropy integrand, S^{or}, and the mean square deviation $[\mathrm{MSD}=(1/N)\Sigma(g^{\mathrm{exact}}-g^{\mathrm{approx}})^2]$ between the true and the approximate distribution. The function g^{exact} is calculated from Eq. (12). It is used to obtain the $1d$ and $2d$ marginals, Eqs. (15) and (16). The function g^{approx} is obtained by the factorizations in Table I, normalized to satisfy Eq. (5). We do the calculation for $r=2.8$ and 3.2 Å. In addition, we evaluate the ODF using a distance dependent dielectric $(\epsilon=r)$[67] for the electrostatic interactions of the TIP4P potential [Eq. (13)] to test the robustness of the factorizations. This provides a check as to whether the factorizations would perform similarly for a potential that approximates some aspects of the potential of mean force in the liquid. The exact U^{or} and S^{or} are also given in the table.

TABLE II. Performance of the factorizations in the gas.

	$r=2.8$ Å			$r=3.2$ Å			$r=2.8$ Å, $\epsilon=r$		
	$-U^{\mathrm{or}}$	$-S^{\mathrm{or}}$	MSD	$-U^{\mathrm{or}}$	$-S^{\mathrm{or}}$	MSD	$-U^{\mathrm{or}}$	$-S^{\mathrm{or}}$	MSD
Exact	4.89	2.73		3.44	1.83		6.52	3.49	
$F1$	2.68	1.82	6.7	2.31	1.19	2.21	3.55	2.63	13.9
$F2$	4.95	3.62	24.7	3.46	2.47	6.58	6.97	4.93	88.2
$F3$	3.59	2.13	3.17	2.63	1.36	1.18	6.09	3.26	2.60
$F4$	0.22	1.65	5.55	0.64	0.84	2.40	0.14	2.88	6.44
$F5$	3.89	2.23	3.65	2.80	1.44	1.31	5.93	3.20	5.49
$F6$	2.05	1.75	5.34	1.37	0.91	2.30	3.44	2.82	8.09
$F7$	4.27	2.62	6.15	2.98	1.66	2.03	6.22	3.54	9.58
$F8$	4.95	3.32	7.83	3.55	2.41	3.68	6.58	3.87	6.41

From Table II we see that $F1$, $F4$, $F6$ are clearly inadequate and that $F3$ and $F5$ are better. $F2$ predicts energies and entropies that are somewhat too large and also has a very high MSD value. It should be noted also that it does not have the correct behavior in the limit when the angles are uncorrelated. It is interesting that even with such a high MSD, the error in the energies and entropies is not very large. The reason for the overestimation of the magnitude of the energies and entropies by $F2$ is that in this factorization each of the 4 angles $\theta_1,\theta_2,\chi_1,\chi_2$ appears twice and this makes the factored ODF too structured. In $F7$ this is remedied by dividing by the four $1d$ marginals. $F7$ gives good results for the energy and entropy, although they are somewhat smaller in magnitude than the correct values. In addition, the MSD value is satisfactory, although not the smallest in the table. It is possible to identify other factorizations that will give better results for the energy or the entropy individually (e.g., $F2$ for the energy), but it is difficult to find ones that work well for both. $F8$ is a superpositionlike approximation, consisting of all possible pairs of $2d$ marginal distributions. Compared to $F7$, it gives better results for the energy, worse results for the entropy, and higher MSD for dielectric equal to 1. Since entropy is of primary interest in this work and due to its simplicity, $F7$ was chosen for application to liquid water.

For $F7$ we recalculated all $1d$ and $2d$ marginals [Eqs. (15) and (16) but with the approximate g under the integral] and found them to be in almost quantitative agreement with the original marginals (results not shown). Thus $F7$ is self-consistent and we conclude that it is a reasonable approximation. Since the structure of the ODF is similar in the gas and in the liquid, this factorization should be reasonable for the liquid ODF, and it is used in Sec. IV B for liquid water. It is likely that, since this factorization underestimates somewhat the magnitude of the energy and entropy in the gas (by about 13% and 5%, respectively), it will also do so in the liquid. As one test of this approximation, we calculated the OH and HH site–site distribution functions from $F7$ and compared them to those obtained directly from the Monte Carlo simulation [Figs. 12(a) and 12(b)]. There is satisfactory agreement between the calculated and the exact distribution functions.

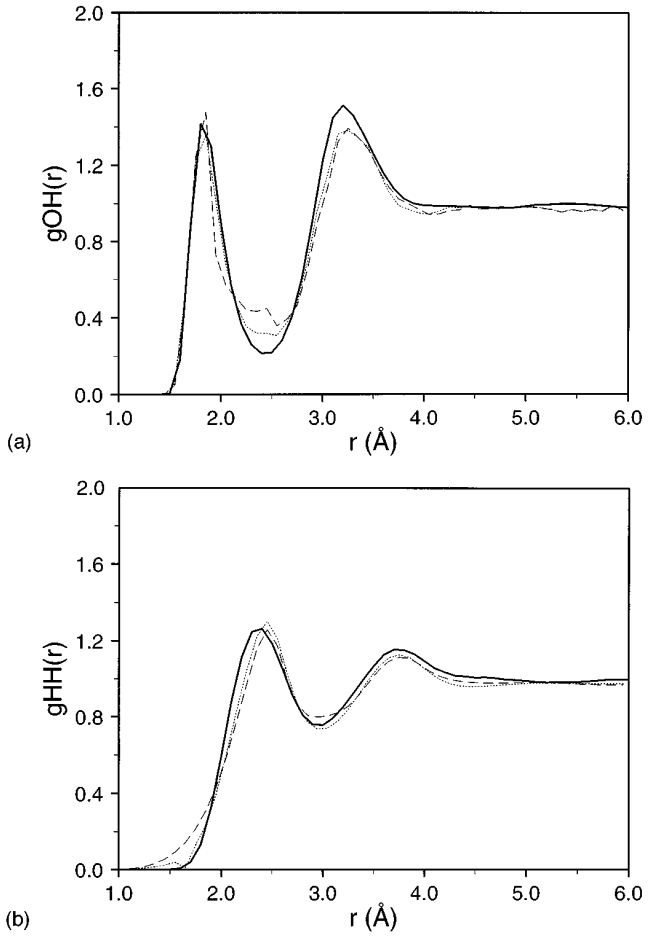

FIG. 12. Site–site correlation functions directly from the simulation (solid line), from factorization $F7$ (dashed line), and from the AGP approximation (dotted line). (a) OH correlation function, (b) HH correlation function.

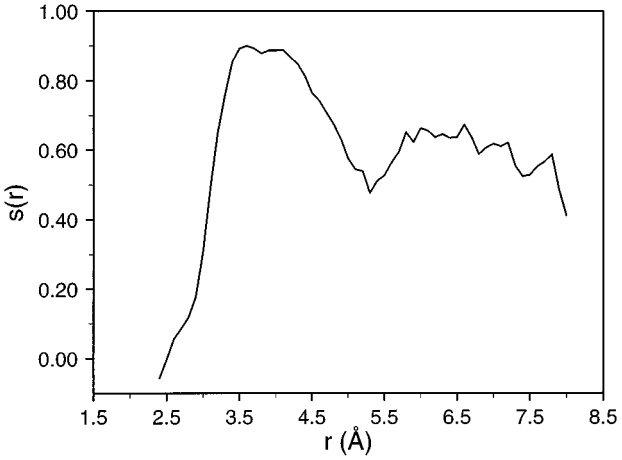

FIG. 13. The smoothing function $s(r)$ used in the AGP approximation.

C. Adjusted gas-phase orientational distribution

The second approach to obtaining the ODF in the liquid is to use the gas-phase ODF as a basis and to modify it by using available information from the liquid state simulations. This information includes the calculated marginal distributions in the 1st subshell, the 2nd subshell and the 2nd neighbor shell and the orientationally averaged interaction energy.

We assume that the effect of the liquid state will be an overall ''smoothing'' of the orientational correlation function

$$g^s(\omega^2|r)=g^{\mathrm{gas}}(\omega^2|r)+s(r)(1-g^{\mathrm{gas}}(\omega^2|r)). \tag{28}$$

The smoothing coefficient $s(r)$ for each distance r can be determined by requiring that g^s reproduces the U^{or} calculated from the simulation. This condition leads to an equation for $s(r)$ of the form

$$s(r)=\frac{U^{\mathrm{or}}[r;\mathrm{simul}]-U^{\mathrm{or}}[r;g^s]}{\langle U\rangle_r-U^{\mathrm{or}}[r;g^s]}, \tag{29}$$

where $\langle U\rangle_r$ is an unweighted average over orientations $[(1/\Omega^2)\int u(r,\omega^2)d\omega^2]$. The function $s(r)$ calculated with Eq. (29) is shown in Fig. 13. The greatest degree of smoothing is required around the first minimum of the RDF, where s takes values as high as 0.85. The assumption of uniform smoothing is an approximation. Packing interactions in the liquid state can enhance or reduce selectively the probability of certain orientations, as found in comparison of the marginal distributions in the gas and in the liquid.

One way of adjusting the smoothed gas-phase ODF [g^s in Eq. (28)] to make it consistent with the marginal distributions obtained by simulation is to use the expression

$$\begin{aligned} g^{\mathrm{AGP}}(\theta_1,\theta_2,\phi,\chi_1,\chi_2|r) &= g^s(\theta_1,\theta_2,\phi,\chi_1,\chi_2|r)*\delta g(\theta_1,\theta_2|r) \\ &\quad *\delta g(\chi_1,\chi_1|r)*\delta g(\phi|r), \end{aligned} \tag{30}$$

where

$$\delta g(\theta_1,\theta_2|r)=g^{\mathrm{liq}}(\theta_1,\theta_2|r)/g^s(\theta_1,\theta_2|r), \tag{31}$$

and so on, $g^s(\theta_1,\theta_2|r)$ is the marginal orientational distribution obtained from g^s [Eq. (28)] and $g^{\mathrm{liq}}(\theta_1,\theta_2|r)$ is the true liquid phase marginal distribution obtained from the simulation. With g^{AGP} (AGP stands for adjusted gas phase) we can calculate a new U^{or} and compare it with that from the simulation. This U^{or} is somewhat more negative than the correct one at short distances and less negative at longer distances [see Fig. 3(b)]. As a result, the molar energy calculated from this approximate U^{or} is slightly more negative than that from the simulation. This small discrepancy in U^{or} is tolerable considering the gain of consistency with the computed marginal distributions, which should yield an improved value for the entropy that is our primary concern.

We have tested the self-consistency of g^{AGP} by calculating its marginals and comparing them to those obtained from the simulation. In general, the $1d$ and $2d$ marginals were quite similar to those obtained from simulation. The ϕ distribution is flat, as observed in the simulation. In the 2nd shell the distributions are relatively flat and so they do not contribute much to the entropy, as is shown below. We also calculated the OH and HH site–site distribution functions,

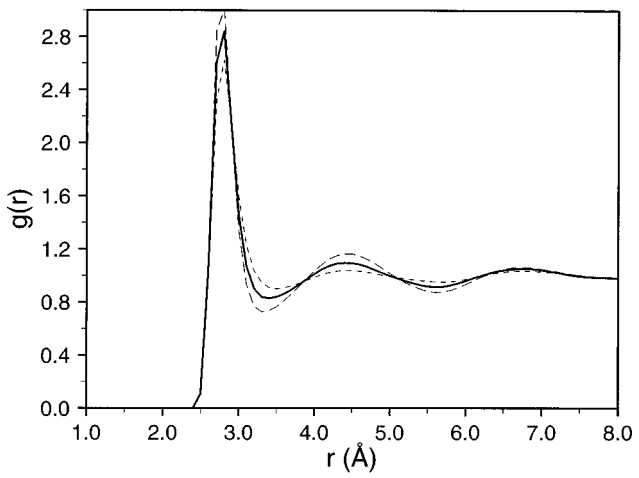

FIG. 14. The radial distribution function at different temperatures: 25 °C (solid line), 5 °C (long dashed line), and 65 °C (short dashed line).

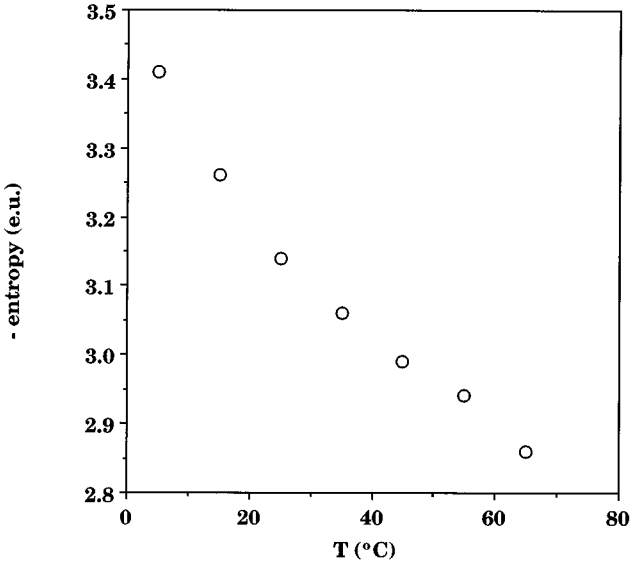

FIG. 15. Translational correlation entropy in water as a function of temperature.

which, as in the case of factorization $F7$, are in satisfactory agreement with the exact distributions from the simulation [see Figs. 12(a) and 12(b)].

IV. RESULTS FOR THE ENTROPY AND HEAT CAPACITY

The translational contribution is calculated from the RDF as a function of temperature in Sec. IV A. The results for the orientational entropy are presented in Sec. IV B from the factorization approximations, and in Sec. IV C from the adjusted gas-phase approximation. Section IV D presents the results for high pressure.

A. Translational entropy

The entropy due to correlations in the positions of the molecules (translational correlation entropy) is given by Eq. (7) and can be readily evaluated from the RDF determined in the simulations. The temperature dependence of the RDF is shown in Fig. 14. As the temperature increases, the RDF becomes flatter. The results for the translational entropy as a function of temperature are shown in Fig. 15. The value at 25 °C is -3.14 e.u. For comparison, the translational entropy in the Lennard-Jones fluid at similar density and reduced temperature (kT/ϵ) equal to 1.15 is about -7 e.u.[47] The value for water is smaller due to the fact that the RDF for a Lennard-Jones system exhibits stronger and longer-ranged oscillations than the water RDF (compare Fig. 14 to Fig. 3 of Ref. 47). The origin of this difference can be traced to the characteristic open structure of water. For example, the reduced height of the first peak of the RDF reflects the fact that water has fewer nearest neighbors (about 5) than simple fluids at similar density. Furthermore, the need for tetrahedral arrangement of the molecules cannot be accommodated by the layerlike packing which gives rise to the second and higher peaks in the RDF of simple fluids. Thus, in terms of radial correlations, water is less structured than a Lennard-Jones liquid. The highly structured nature of water is reflected in the angular correlation function. This correlation is lost when an average over angles is performed to obtain the RDF.

To obtain the heat capacity contribution C_p^{tr} corresponding to the translational entropy, we use a least squares fit of the results to the Taylor expansion of the translational entropy around a reference temperature To (with To=298.15)

$$S(T)-S(\mathrm{To})=\frac{\mathrm{Cp(To)}}{\mathrm{To}}*(T-\mathrm{To}) + \frac{1}{2\mathrm{To}}\left\{\left(\frac{d\mathrm{Cp}}{dT}\right)_{\mathrm{To}}-\frac{\mathrm{Cp(To)}}{\mathrm{To}}\right\}*(T-\mathrm{To})^2. \tag{32}$$

The value of C_p^{tr} is found to be 3.15 e.u. at To.

B. Orientational entropy from factorizations

A number of factorizations have been applied to the calculation of the orientational entropy in liquid water. They include those in Table I and some others not shown. Here, we report the results for the one considered to be best overall based on the gas phase results, namely $F7$ in Table I. The behavior of the factorizations in the gas carries over to the liquid; i.e., factorizations which give similar values for the entropy in the gas, also give similar values for the entropy in the liquid and those that underestimate the energy in the gas also underestimate it in the liquid. The results at 25 °C are given in Table III.

Figure 16 shows the calculated energy from $F7$ and the exact energy from the simulation as a function of temperature. The factorization underestimates the magnitude of the energy by 16%, which is consistent with the fact that it underestimates the magnitude of the energy in the gas by a

TABLE III. Results for the energy, entropy, and heat capacity of liquid water at 25 °C.[a,b]

		Factorization $F7$	AGP
Excess energy, simulation	-10.0, -10.1[c]		
Excess energy, $g(r,\omega)$		-8.3 ± 0.25	-10.1 ± 0.20
Translational $2p$ entropy	-3.14 ± 0.02		
Orientational $2p$ entropy		-9.1 ± 0.20	-11.7 ± 0.15
Total $2p$ entropy		-12.2 ± 0.20	-14.8 ± 0.15
Excess entropy of TIP4P, simulation	-15.2		
Excess entropy of water, experimental	-14.1		
Excess Cp from energy, simulation		17.1	16.3
Excess Cp from energy, $g(r,\omega)$		15.8	19.2
Excess Cp from $2p$ entropy			
Translational	3.15		
Orientational		13.8	15.7
Total		17.0	18.9
Excess Cp of water (exp)	12.0		

[a]Energies in kcal/mol, entropies, and heat capacities in cal/mol K (e.u.).
[b]Uncertainties pertain to statistical error for the marginal distribution functions obtained by simulation.
[c]Two different sets of simulations.

similar amount. The slope of the two lines is very similar. A least squares fit to the Taylor expansion of the energy around To=298.15 K

$$E(T)-E(\mathrm{To})=\mathrm{Cp}(\mathrm{To})*(T-\mathrm{To})+\frac{1}{2}\left(\frac{d\mathrm{Cp}}{dT}\right)_{\mathrm{To}}*(T-\mathrm{To})^2 \tag{33}$$

gives Cp=17.1 from the simulation data and Cp=15.8 from the factorization at To=298.15 K.

It is possible to identify factorizations that give essentially the exact energy in the gas phase (e.g., $F2$ in Table II), and which would perform better in the liquid, if we relaxed the requirement that the same factorization also perform well for the entropy. Since this factorization is otherwise not as good as $F7$, the result for the energy is apparently due to a fortuitous cancellation of error.

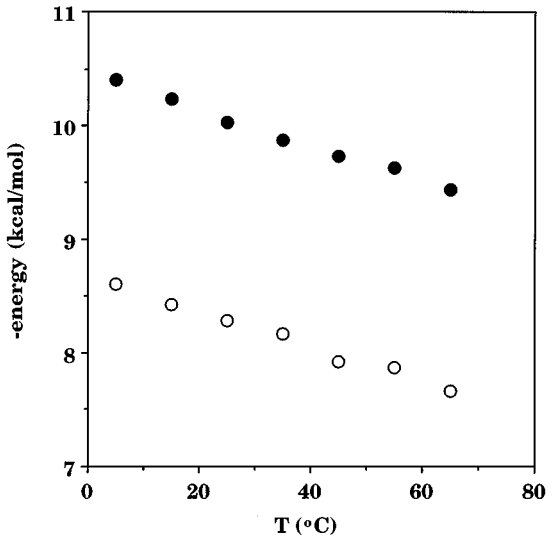

FIG. 16. Excess molar energy in the liquid from the simulation (filled circles) and from factorization $F7$ (empty circles) as a function of temperature.

The orientational entropy is calculated from Eqs. (8) and (9). The ODF needed in Eq. (9) is approximated by the factorizations of Table I using the marginal distributions obtained from the MC simulations. These are calculated over three discrete regions of r (see Sec. II), and an average value of S^{or} within these regions is obtained. Figure 17 shows the calculated orientational entropy from $F7$ as a function of temperature. At 25 °C the value is -9.1 e.u., which, when added to the translational entropy (-3.14 e.u.) gives -12.24 e.u. The excess entropy of TIP4P water extracted from free energy simulations by subtracting the molar energy from the excess chemical potential is -15.2 e.u.[68] and is close to the experimental value, which is -14.1 e.u.[69] We note that the excess entropy ($s^{\mathrm{ex}}=s-s^{\mathrm{id}}$) is related to Ben-Naim's solvation entropy $\Delta S^*(-\partial\mu/\partial T)$ through the equation $s^{\mathrm{ex}}=\Delta S^*-k(1-T\alpha)$, where α is the thermal expansion coefficient. The difference is due to the fact that $\partial\mu^{\mathrm{id}}/\partial T=s^{\mathrm{id}}-k(1-T\alpha)$.

The contribution of the orientational entropy to the heat capacity is 13.8 e.u. which when added to the translational entropy contribution gives 17 e.u. This value is within statistical uncertainty of the value obtained from the variation of the energy with temperature (15.8 e.u., see above). Thus, the approach is thermodynamically consistent. Addition of the ideal contribution ($3R$) gives a total calculated heat capacity of 23 e.u. The experimental value for water is 18 e.u. Part of the discrepancy can be eliminated by including a quantum correction for Cp (about -2.2 e.u.).[70]

Equation (8) allows a decomposition of the orientational entropy into contributions from different regions of r. At all temperatures, the major contribution to the orientational entropy comes from the first neighbor shell (93%), which reflects the fact that orientational correlations are strongest in this shell. In this section we have neglected any contributions to the orientational entropy from beyond the second shell. These contributions are calculated in the AGP approximation (next section) and are found to be very small.

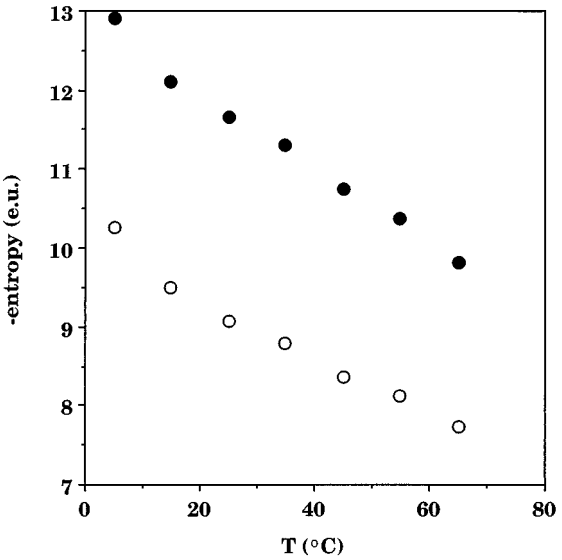

FIG. 17. Orientational correlation entropy in the liquid from factorization $F7$ (empty circles) and from the AGP approximation (filled circles) as a function of temperature.

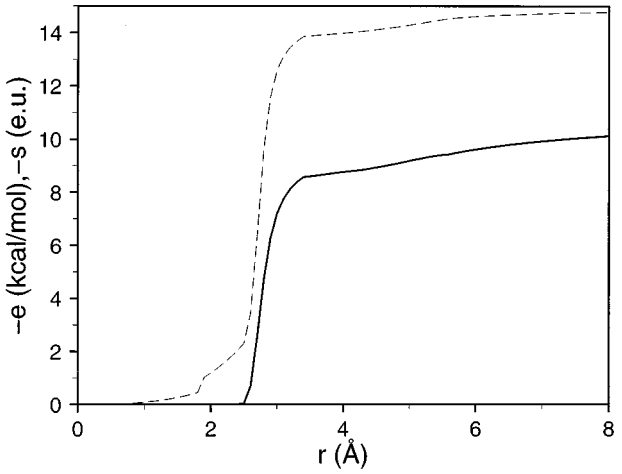

FIG. 18. Cumulative integral for the energy (solid line) and the entropy (dashed line) in the AGP approximation at 25 °C.

C. Orientational entropy from the adjusted gas phase approximation

For the calculation of the orientational entropy in the AGP approximation we use Eqs. (8) and (9) with $g(\omega^2|r)$ from Eq. (30). The orientational entropy integrand, S^{or}, in the AGP approximation is shown in Fig. 4, along with that in the gas phase. It is slightly larger in magnitude than that in the gas phase at short distances (perhaps due to the enhancement of tetrahedrality) and significantly smaller at intermediate distances. The ''kink'' in this figure [as well as in Fig. 3(b)] at 3.4 Å is an artifact of using marginals averaged over discrete regions of r (2.8–3.4 and 3.4–5.6 Å).

The orientational entropy calculated from this approximation as a function of temperature is shown in Fig. 17. The value at 25 °C is −11.65 e.u. (see Table III), somewhat more negative than that obtained from the factorization. When added to the translational contribution (−3.14 e.u.), the AGP value gives −14.8 e.u., which agrees well with the entropy of TIP4P water obtained by free energy simulations (−15.2 e.u.). From the slope of the curve in Fig. 17 we obtain a contribution of 15.7 e.u. to Cp, which, along with the translational contribution gives Cp=18.9 e.u. The Cp obtained from the energy curve is 16.3 e.u. [The value is slightly different from 17.1 e.u. given above because a different set of simulations was used. The difference between the two values is an indication of the statistical uncertainty in the calculation of Cp from simulations].

Figure 18 shows the cumulative integral of the total entropy (translational and orientational) as a function of the upper integration limit. About 94% of the total entropy comes from the first neighbor shell ($r \leqslant 3.4$ Å) and another 4% from the second neighbor shell. The corresponding numbers for the energy (from the approximate ODF) are 85% and 8%. This behavior contrasts to that of the dielectric properties, which have large contributions from distant regions.[33,71] Apparently, the dominance of short range interactions and correlations for energies and entropies carries over to solutes and is an important reason for the high accuracy of simulations for the calculation of solvation free energies in water.

If the liquid ODF had been approximated by the gas-phase ODF [i.e., if Eq. (22) has been adopted], the orientational entropy would be −23 e.u., twice as large as the above value, and the excess molar energy −19 kcal/mol, almost twice as large as the true value. Thus, although the liquid and gas-phase ODF exhibit significant similarities, Eq. (22) is not an accurate approximation.

D. Effect of high pressure

The change in entropy with volume is given by the thermodynamic relation

$$\left(\frac{\partial s}{\partial v}\right)_T = \left(\frac{\partial P}{\partial T}\right)_V = \frac{\alpha}{\kappa}, \tag{34}$$

where α is the thermal expansion coefficient and κ the isothermal compressibility. For water at 20 °C, $\alpha = 257.21\times10^{-6}$ K^{-1} and $\kappa = 45.2472\times10^{-6}$ bar^{-1} (Ref. 72), which gives $\alpha/\kappa = 0.0824$ cal/(mol K Å^3). Due to the very small value of the thermal expansion coefficient of water (it actually becomes negative below 4 °C) this ratio is atypically small. For example, for CCl_4 at 20 °C, $\alpha = 1236\times10^{-6}$ K^{-1} (Ref. 73), $\kappa = 106.8\times10^{-6}$ bar^{-1} (Ref. 72), and $\alpha/\kappa = 0.168$ cal/(mol K Å^3), twice as large as the value for water.

We can use Eq. (2) for the entropy to evaluate the derivative in Eq. (34):

$$\frac{\partial s}{\partial v} = \frac{\partial s^{\mathrm{id}}}{\partial v} + \frac{\partial s^{\mathrm{ex}}}{\partial v}. \tag{35}$$

For a rigid water molecule

$$s^{\mathrm{id}} = \tfrac{8}{2}k - k \ln \frac{\Lambda^3}{v q^{\mathrm{rot}}}, \tag{36}$$

where q^{rot} is the rotational partition function. Since the volume derivative of the ideal contribution is

$$\frac{\partial}{\partial v}(k \ln \mathbf{v}) = \frac{k}{v} = 0.066 \ \text{cal/mol K Å}^3, \tag{37}$$

the derivative of the excess entropy is 0.0164 cal/mol K Å^3. The volume derivative of the two-particle term in the entropy expression has two contributions: one from the change in density and one from the change in the PCF with volume

$$\left(\frac{\partial s^{(2)}}{\partial v}\right)_T = \left\{-\frac{s^{(2)}}{v}\right\} + \left\{-\frac{1}{2} k \frac{\rho}{\Omega^2}\left(\frac{\partial I}{\partial v}\right)_T\right\}, \tag{38}$$

where

$$I = \int [g^{(2)} \ln g^{(2)} - g^{(2)} + 1] d\mathbf{r}\, d\omega^2.$$

Since $s^{(2)} \approx -15$ e.u. and $v \approx 30$ Å^3, the first term is positive and equal to about 0.5 cal/(mol K Å^3). This means that the second term is large and negative, which requires that

$$\left(\frac{\partial I}{\partial v}\right)_T > 0. \tag{39}$$

[The coefficient of this term in Eq. (38) is of the order 10^{-4} e.u./Å^3]. Consequently, correlations must increase with an increase in volume, or decrease with an increase in density. This appears counterintuitive, since in simple fluids compression leads to sharpening of the intermolecular correlations. The reason that this is not true for water at room temperature and 1 atm is its open tetrahedral structure. Compression leads to partial destruction of this tetrahedral order and a concomitant decrease in orientational correlations.

This reasoning is supported by the results of the high pressure MC simulation. These simulations were run at 25 °C and 10 000 atm pressure. The molar volume decreased from 30.1 Å^3 at 1 atm to 23.75 Å^3 at 10 000 atm (corresponding to 1.26 g/cm^3). If we assume that the compressibility does not vary much with pressure, a rough estimate of it is

$$\kappa = -\frac{1}{v}\left(\frac{\partial v}{\partial P}\right)_T \approx -\frac{1}{\langle v \rangle}\frac{\Delta v}{\Delta P} \approx 23 \times 10^{-6} \ \text{bar}^{-1}. \tag{40}$$

This value is of the same order as obtained previously for the TIP4P model by analysis of density fluctuations[74] and is smaller by a factor of 2 than the experimental compressibility of water given above.

Figure 2 shows the O–O RDF at high pressure. Compared to the low pressure RDF, this curve has a diminished first peak and the first minimum moved out to 4.5 from 3.4 Å at low pressure. This behavior at high pressure has been observed in previous simulations using the TIP4P model[74–76] and other water models[77–80] as well as in x-ray diffraction experiments.[81] This change in the shape of the RDF reflects the increased packing efficiency that liquid water achieves at high pressure. It results from ''pushing'' next-nearest neighbors closer to the central water molecule from ''antitetrahedral'' directions.[74]

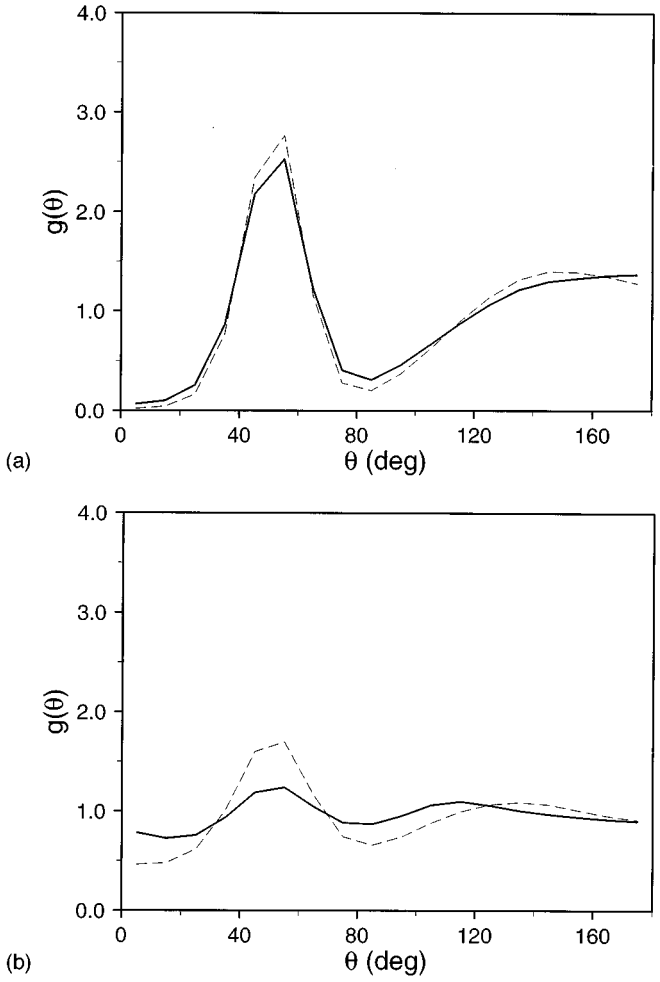

FIG. 19. $g(\theta)$ in the liquid at 25 °C and $P = 10\,000$ atm (solid line) compared to that at $P = 1$ atm (dashed line). (a) First subshell, (b) second subshell.

Figures 19 and 20 show the θ and χ marginals in the first and second subshells (these designations refer to the 1 atm RDF) together with the corresponding results at 1 atm. There is a clear flattening of the correlation functions, especially in the second subshell. This appears to be in conflict with conclusions based on neutron diffraction experiments on liquid water at high pressure.[82,83] The experiments were interpreted as showing an increase in correlations in both positions and orientations of the water molecules with pressure. This inference was based on the observed increase in the amplitude of the oscillations of the calculated neutron-weighted correlation function in the range 3.5–5 Å. The neutron-weighted correlation function is a weighted combination of the three site–site correlation functions (with the OH and HH function making the dominant contribution)[82,83] and thus is difficult to interpret. It is possible that a decrease in the oscillations in some of the site–site functions may appear as an increase in the oscillations of the neutron-weighted function. Monte Carlo simulations, which reproduce the neutron-weighted

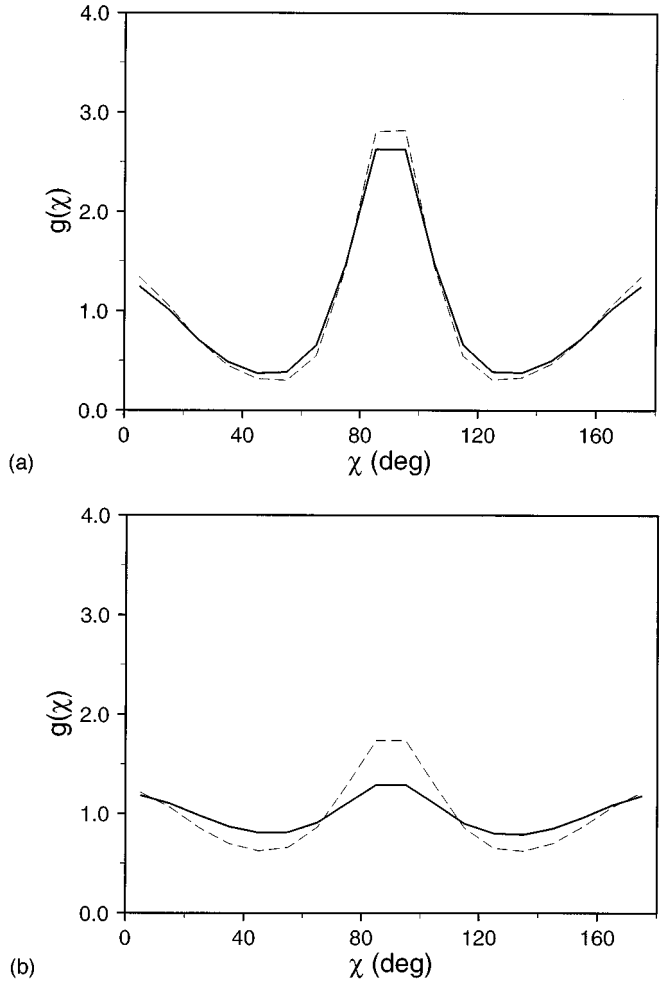

FIG. 20. $g(\chi)$ in the liquid at 25 °C and $P=10\,000$ atm (solid line) compared to that at $P=1$ atm (dashed line). (a) First subshell, (b) second subshell.

function[74,78] give site–site functions that do not reveal any enhancement of orientational correlations. In fact, the first OH peak, reflecting hydrogen bonding, slightly decreases and the HH function flattens out with increasing density.[74–76] For a more direct comparison it is important to obtain the separate OO, OH, and HH correlation functions from neutron diffraction experiments, which is possible with isotopic substitution.[84] Although site–site functions are very informative, they are still not straightforward to interpret because they depend on both translational and orientational correlations. The most unambiguous measure of orientational correlations is obtained from angular distributions functions, such as those calculated here, which, unfortunately, cannot be obtained experimentally. It should be noted that the decrease of orientational correlations with increased density applies to TIP4P water at room temperature and ambient pressure. It is possible that for other conditions an increase in density enhances orientational correlations. This seems to be the case in water above its boiling point.[84]

Calculation of the entropy with the $F7$ factorization reflects this reduction in the correlations. Whereas the translational entropy decreases from -3.1 e.u. at 1 atm to -4.0 e.u. at 10 000 atm, the orientational entropy increases from -9.1 to -7.6 e.u. The total excess two-particle entropy at high pressure is -11.6 e.u., compared to -12.2 e.u. at low pressure. Thus the change in two particle entropy from 1 to 10 000 atm is estimated to be $+0.6$ e.u. Since the change in the ideal part of the entropy is $k\ln(\mathbf{v}_1/\mathbf{v}_{10\,000})=-0.5$ e.u., the model predicts Δs from 1 to 10 000 atm to be slightly positive $(+0.1)$ instead of slightly negative. The experimental estimate, if α/κ is assumed to be constant in this pressure range, is $\Delta s=0.0824^{*}(-6.35\ \text{Å}^3)=-0.52$ e.u. The uncertainties arising from the approximations in the theory and the calculations and from the inherent limitations of any empirical potential for water are such that the model does not reproduce the subtle changes in entropy with density. However, the theory clearly explains the small value of the volume derivative of the entropy in water by the fact that increase in density reduces orientational correlations. Below 4 °C, the thermal expansion coefficient [and therefore the volume derivative of the entropy, see Eq. (34)] becomes negative, apparently because the reduction in orientational correlations with density dominates the increase in translational correlations.

V. CONCLUDING DISCUSSION

The goal of this work was to obtain a better understanding of the excess entropy of liquid water. For this purpose a correlation function expansion was used, truncated at the two-particle level. The two-particle term was separated into a translational and an orientational contribution. The translational contribution can be calculated directly from the radial distribution function, which is easily obtained from simulations. By contrast, the orientational contribution depends on the angular distribution function which is a function of five angles and so is very difficult to obtain from simulations. To overcome this problem, we have introduced various approximations for the angular distribution function that are based either on the low density limit, modified by liquid state marginal distribution functions obtained from simulations, or on a factorization of the angular distribution function in terms of these lower dimensionality marginal distribution functions. The translational and orientational contributions calculated in this way are compared with experimental values. The comparison indicates that the excess entropy and heat capacity of water are dominated by the two-particle term; the sum of the higher order terms makes a relatively small contribution (of the order of 3% to 20%, depending on the approximation used for the ODF). Further, it is shown that the two-particle contribution to the excess entropy of TIP4P water consists of a translational contribution of -3.14 e.u. and an orientational contribution of between -9.1 and -11.65 e.u. at 25 °C and 1 atm. This gives -12.24 to -14.8 e.u. for the total excess entropy. When the ideal contribution of 30.8 e.u. is added, the absolute entropy of water is calculated to be 16 to 18.56 e.u. These values are to be compared with the experimental values of -14.1 e.u. for the excess entropy and 16.7 e.u. for the absolute entropy. The translational contribu-

tion is smaller than that in simple liquids at similar density. Thus the large magnitude of the excess entropy in water is mostly due to orientational correlations.

The present approach complements other treatments of the entropy of water. The most common method for obtaining the entropy has been to calculate the total free energy by simulations and subtract the internal energy, also calculated by simulation (for example, Refs. 68, 85–87). The results obtained this way for TIP4P and other effective pair potentials are in relatively good agreement with experiment. Calculated values at 25 °C and 1 atm are between −12 and −16 e.u. The entropy of water has also been calculated by the adiabatic switching method using computer simulations.[88] The value obtained for the excess entropy at 303 K was about −13.5 e.u.

Calculation of the thermodynamics of liquid water have also been performed based on integral equation theories.[16,89,90] Here, too, the approach has been to calculate first the free energy and subsequently the entropy either by subtraction of the internal energy[16,90] or by a temperature derivative of the free energy.[89] The values obtained for the entropy depend on the closure and the details of the calculation. Yu *et al.*[89] using the HNC-RISM equation and a model similar to TIP3P obtained the value −24.5 e.u. for the excess entropy, significantly more negative than both the experimental value and the theoretical values obtained by free energy simulations. With the same theory but a modified potential Lue and Blankschtein[90] obtained a value (−15.6 e.u.) much closer to experiment, perhaps because the OH repulsion parameter was adjusted to reproduce the experimental internal energy of water. More recently, the diagramatically proper integral equation of Chandler–Silbey–Ladanyi was applied to liquid water and gave values of the order of −19 to −20 e.u. for common water models.[16] It should be mentioned for completeness that there have been numerous calculations of the entropy with simplified statistical mechanical models for water, such as the mixture model,[91] the cell model,[92] the random network model,[93] and various lattice models.[94,95] These models involve assumptions or simplifications that limit their reliability.

Although the free energy simulation methods provide, in principle, more accurate results than the approach described here, the present treatment has made it possible to obtain more insights into the origins of the excess entropy of water. The significance of the interpretation depends on the accuracy of the approximations used for the ODF. These approximations have been shown to be consistent with the site-site distribution functions and with the one and two dimensional marginal distributions obtained from the simulation. The various factorizations that reproduce the gas-phase entropy give similar values for the orientational entropy in the liquid. Further, the very different AGP approximation also gives similar results. However, more work is needed to better characterize the ODF. One approach is to calculate three-variable angular marginal distributions. Special care is needed for the region around the first minimum of the RDF, where the largest differences in the orientationally averaged energy exist between the gas and the liquid. This is the region that contains contributions from nontetrahedrally coordinated water (the ''interstitial'' water described by Svishchev and Kusalik[34] and discussed by Stanley and co-workers[96]). In this region packing effects are likely to be most important and the present approximate ODFs are not refined enough to include the small interstitial maximum observed by these authors; one would need distribution functions at a finer distance grid. However, these structural features are expected to have only a small effect on the thermodynamic functions because they are quite weak compared to the major structural features (tetrahedral hydrogen bonding, see Fig. 3 of Ref. 34). They are likely to have a more important effect on dynamic properties of water, such as the viscosity and the diffusion coefficient.

The fact that two-particle correlations appear to make the dominant contribution to the excess entropy of water does not mean that triplet correlations are not important in the structure of the liquid. For example, Hummer and Soumpasis[29] found that the water hydrogen and oxygen density distribution on the liquid side of an ice–water interface cannot be reproduced unless triplet correlations are included. Although the condition $\delta g^{(3)}=1$ is sufficient for the two-particle term to be dominant, it is not necessary. This function can deviate substantially from unity at all points and still the integral over it may be small. Another possibility is that higher order terms, such as three-particle and four-particle terms, approximately cancel. In any case, higher order terms seem to make relatively small contributions (of the order of 10%) to the thermodynamic properties of all liquids studied so far, including water. If this is universal, the second-order entropy affords a practical route for obtaining the chemical potential of dense fluids, since the energy is straightforward to calculate by simulation.

The temperature dependence of the two-particle entropy and of the energy calculated by the present approximations give reasonable values for the heat capacity that agree within their statistical uncertainty. This indicates that the truncated entropy expansion, Eq. (2), is equally good over the temperature range studied here so that the theory is thermodynamically consistent. The actual value of the calculated heat capacity (23 to 25 e.u.), when the kinetic contribution of $3R$ (for rigid water) has been added, is somewhat larger than the experimental heat capacity of water (~18 e.u.). For a precise comparison with experimental thermodynamic properties, one would have to consider intramolecular contributions and quantum corrections. These have been estimated to be of the order of −2 e.u.[70,97]

The flattening of the two-particle correlation function (hydrogen-bond ''bending'') found in the present calculations is sufficient to produce changes in entropy as a function of temperature consistent with the large heat capacity of water, obviating the need to adopt more complex ''mixture'' type concepts.[98] The dominance of the two-particle term in the entropy suggests that complex collective phenomena involving large numbers of water molecules (like ''flickering clusters''[99]), which imply significant many-body correlations, are not required to interpret the properties of water, at least so far as the entropy is concerned.

The fact that pressure ''breaks'' water structure has been a common explanation for some of the anomalous properties of water[2] but the decrease in orientational correlations with density has not been observed in simulations until now. The small effect of the density on the entropy of water is qualitatively reproduced by the entropy calculations.

As already mentioned, the study of two TIP4P molecules in the gas phase was not intended to represent the true water dimer. The TIP4P potential is an effective pairwise potential developed for liquid state simulations and is more polarized than gas phase molecules. However, the methodology used here, along with a realistic pairwise potential for water in the gas phase, could be used to determine thermodynamic properties of the vapor phase. Particularly interesting would be the calculation of equilibrium constants for water dimer formation, which are important in atmospheric chemistry. Usually, these calculations are carried out by harmonic vibrational analysis of the global energy minimum.[100]

ACKNOWLEDGMENTS

This work was supported in part by a grant from the National Science Foundation. The calculations were carried out on HP9000/735 workstations and a Convex 220 computer. We thank Peter Kusalik for carefully reviewing the manuscript and providing many helpful comments. He also suggested factorization $F8$.

[1] J. D. Bernal and R. H. Fowler, J. Chem. Phys. **1**, 515 (1933).
[2] D. Eisenberg and W. Kauzmann, *The Structure and Properties of Water* (Oxford University, New York, 1969).
[3] H. S. Frank and A. S. Quist, J. Chem. Phys. **34**, 604 (1961).
[4] M. Vedamuthu, S. Singh, and G. W. Robinson, J. Phys. Chem. **98**, 2222 (1994).
[5] J. Pople, Proc. R. Soc. London, Ser. A **205**, 163 (1951).
[6] M. G. Sceats, M. Stavola, and S. A. Rice, J. Chem. Phys. **70**, 3927 (1979).
[7] A. R. Henn and W. Kauzmann, J. Phys. Chem. **93**, 3770 (1989).
[8] C. G. Gray and K. E. Gubbins, *Theory of Molecular Fluids* (Clarendon, Oxford, 1984).
[9] J. P. Hansen and I. R. McDonald, *Theory of Simple Liquids* (Academic, London, 1986).
[10] I. Z. Fisher and B. L. Kopeliovich, Soviet Phys. Dokl. **5**, 761 (1961).
[11] P. Attard, J. Chem. Phys. **91**, 3072 (1989).
[12] D. Chandler and H. C. Andersen, J. Chem. Phys. **57**, 1930 (1972).
[13] D. Chandler, R. Silbey, and B. M. Ladanyi, Mol. Phys. **46**, 1335 (1982).
[14] B. M. Pettitt and P. J. Rossky, J. Chem. Phys. **77**, 1451 (1982).
[15] D.-M. Duh, D. N. Perera, and A. D. J. Haymet, J. Chem. Phys. **102**, 3736 (1995).
[16] L. Lue and D. Blankschtein, J. Chem. Phys. **102**, 5427 (1995).
[17] F. H. Stillinger, Adv. Chem. Phys. **31**, 1 (1975).
[18] O. Matsuoka, E. Clementi, and M. Yoshimine, J. Chem. Phys. **64**, 1351 (1976).
[19] W. L. Jorgensen, J. Chandrasekhar, J. D. Madura, R. W. Impey, and M. L. Klein, J. Chem. Phys. **79**, 926 (1983).
[20] H. J. C. Berendsen, J. R. Grigera, and T. P. Straatsma, J. Phys. Chem. **91**, 6269 (1987).
[21] J. Caldwell, L. X. Dang, and P. A. Kollman, J. Am. Chem. Soc. **112**, 9144 (1990).
[22] D. N. Bernardo, Y. Ding, K. Krogh-Jespersen, and R. M. Levy, J. Phys. Chem. **98**, 4180 (1994).
[23] A. Rahman and F. H. Stillinger, J. Chem. Phys. **55**, 3336 (1971).
[24] W. L. Jorgensen, J. Am. Chem. Soc. **103**, 335 (1981).
[25] A. H. Narten, J. Chem. Phys. **56**, 5681 (1972).
[26] A. K. Soper and M. G. Phillips, Chem. Phys. **107**, 47 (1986).
[27] E. A. Muller and K. E. Gubbins, Mol. Phys. **80**, 91 (1993).
[28] A. Baranyai and D. J. Evans, Phys. Rev. A **42**, 849 (1990).
[29] G. Hummer and D. M. Soumpasis, Phys. Rev. E **49**, 591 (1994).
[30] O. Steinhauser, Ber. Bunsenges. Phys. Chem. **87**, 128 (1983).
[31] M. Neumann, J. Chem. Phys. **85**, 1567 (1986).
[32] J. Anderson, J. J. Ullo, and S. Yip, J. Chem. Phys. **87**, 1726 (1987).
[33] H. E. Alper and R. M. Levy, J. Chem. Phys. **91**, 1242 (1989).
[34] I. M. Svishchev and P. G. Kusalik, J. Chem. Phys. **99**, 3049 (1993).
[35] P. G. Kusalik and I. M. Svishchev, Science **265**, 1219 (1994).
[36] A. K. Soper, J. Chem. Phys. **101**, 6888 (1994).
[37] H. S. Green, *The Molecular Theory of Fluids* (North-Holland, Amsterdam, 1952).
[38] R. E. Nettleton and M. S. Green, J. Chem. Phys. **29**, 1365 (1958).
[39] T. Morita and K. Hiroike, Prog. Theor. Phys. **25**, 537 (1961).
[40] R. D. Mountain and H. J. Raveche, J. Chem. Phys. **55**, 2250 (1971).
[41] D. C. Wallace, J. Chem. Phys. **87**, 2282 (1987).
[42] D. C. Wallace, Int. J. Quantum Chem. **52**, 425 (1994).
[43] D. C. Wallace, Phys. Rev. A. **39**, 4843 (1989).
[44] A. Baranyai and D. J. Evans, Z. Naturforsch. Teil A **46**, 27 (1991).
[45] B. B. Laird and A. D. J. Haymet, Phys. Rev. A **45**, 5680 (1992).
[46] I. Borzsak and A. Baranyai, Chem. Phys. **165**, 227 (1992).
[47] A. Baranyai and D. J. Evans, Phys. Rev. A **40**, 3817 (1989).
[48] D. C. Wallace, Phys. Rev. A **38**, 469 (1988).
[49] B. B. Laird and A. D. J. Haymet, J. Chem. Phys. **97**, 2153 (1992).
[50] D. C. Wallace, Proc. R. Soc. London, Ser. A **433**, 615 (1991).
[51] B. B. Laird and A. D. J. Haymet, J. Chem. Phys. **100**, 3775 (1994).
[52] T. Lazaridis and M. E. Paulaitis, J. Phys. Chem. **96**, 3847 (1992).
[53] T. Lazaridis and M. E. Paulaitis, J. Phys. Chem. **98**, 635 (1994).
[54] T. L. Hill, *Statistical Mechanics* (McGraw-Hill, New York, 1956).
[55] W. L. Jorgensen, *BOSS, Version 2.8* (Yale University Press, New Haven, 1989).
[56] T. W. Anderson, *An Introduction to Multivariate Statistical Analysis*, 2nd ed. (Wiley, New York, 1984).
[57] J. A. Barker and R. O. Watts, Mol. Phys. **26**, 789 (1973).
[58] C. Pangali, M. Rao, and B. J. Berne, Mol. Phys. **40**, 661 (1980).
[59] T. A. Andrea, W. C. Swope, and H. C. Andersen, J. Chem. Phys. **79**, 4576 (1983).
[60] A. Ben-Naim and F. H. Stillinger, in *Water and Aqueous Solutions*, edited by R. A. Horne (Wiley-Interscience, New York, 1972).
[61] J. G. Kirkwood, J. Chem. Phys. **7**, 911 (1939).
[62] F. H. Stillinger and A. Rahman, J. Chem. Phys. **60**, 1545 (1974).
[63] C. S. Hsu, D. Chandler, and L. J. Lowden, Chem. Phys. **14**, 213 (1976).
[64] N. Quirke and D. J. Tildesley, Mol. Phys. **45**, 811 (1982).
[65] B. M. Ladanyi, T. Keyes, D. J. Tildesley, and W. B. Streett, Mol. Phys. **39**, 645 (1980).
[66] J. M. Haile, Faraday Discuss. Chem. Soc. **66**, 75 (1978).
[67] B. R. Gelin and M. Karplus, Biochemistry **18**, 1256 (1979).
[68] W. L. Jorgensen, J. F. Blake, and J. K. Buckner, Chem. Phys. **129**, 193 (1989).
[69] A. Ben-Naim and Y. Marcus, J. Chem. Phys. **81**, 2016 (1984).
[70] W. L. Jorgensen and J. D. Madura, Mol. Phys. **56**, 1381 (1985).
[71] I. Ruff and D. J. Diestler, J. Chem. Phys. **93**, 2032 (1990).
[72] *CRC Handbook* (CRC, Boca Raton, 1983–84).
[73] *Lange's Handbook of Chemistry* (McGraw-Hill, New York, 1985).
[74] J. D. Madura, B. M. Pettitt, and D. F. Calef, Mol. Phys. **64**, 325 (1988).
[75] M. R. Reddy and M. Berkowitz, J. Chem. Phys. **87**, 6682 (1987).
[76] J. S. Tse and M. L. Klein, J. Phys. Chem. **92**, 315 (1988).
[77] F. H. Stillinger and A. Rahman, J. Chem. Phys. **61**, 4973 (1974).
[78] R. W. Impey, M. L. Klein, and I. R. McDonald, J. Chem. Phys. **74**, 647 (1981).
[79] G. Jancso, P. Bopp, and K. Heinziger, Chem. Phys. **85**, 377 (1984).
[80] K. A. Motakabbir and M. Berkowitz, J. Phys. Chem. **94**, 8359 (1990).
[81] A. V. Okhulkov, Y. N. Demianets, and Y. E. Gorbaty, J. Chem. Phys. **100**, 1578 (1994).
[82] A. Y. Wu, E. Whalley, and G. Dolling, Mol. Phys. **47**, 603 (1982).
[83] M.-C. Bellissent-Funel and L. Bosio, J. Chem. Phys. **102**, 3727 (1995).
[84] P. Postorino, M. A. Ricci, and A. K. Soper, J. Chem. Phys. **101**, 4123 (1994).
[85] J. Hermans, A. Pathiaseril, and A. Anderson, J. Am. Chem. Soc. **110**, 5982 (1988).
[86] M. Mezei, J. Comput. Chem. **13**, 651 (1992).
[87] S.-B. Zhu and C. F. Wong, J. Chem. Phys. **98**, 8892 (1993).
[88] L.-W. Tsao, S.-Y. Sheu, and C.-Y. Mou, J. Chem. Phys. **101**, 3202 (1994).
[89] H.-A. Yu, B. Roux, and M. Karplus, J. Chem. Phys. **92**, 5020 (1990).

[90] L. Lue and D. Blankschtein, J. Phys. Chem. **96**, 8582 (1992).
[91] G. Nemethy and H. A. Scheraga, J. Chem. Phys. **36**, 3382 (1962).
[92] O. Weres and S. A. Rice, J. Am. Chem. Soc. **94**, 8983 (1972).
[93] M. G. Sceats and S. A. Rice, J. Chem. Phys. **72**, 3260 (1980).
[94] G. M. Bell, J. Phys. C **5**, 889 (1972).
[95] P. D. I. Fleming and J. H. Gibbs, J. Stat. Phys. **10**, 351 (1974).
[96] F. Sciortino, A. Geiger, and H. E. Stanley, Nature (London) **354**, 218 (1991).
[97] J. C. Owicki and H. A. Scheraga, J. Am. Chem. Soc. **99**, 7403 (1977).
[98] S. W. Benson and E. D. Siebert, J. Am. Chem. Soc. **114**, 4269 (1992).
[99] H. S. Frank and W.-Y. Wen, Discuss Faraday. Soc. **24**, 133 (1957).
[100] Z. Slanina and J.-F. Crifo, Thermochim. Acta **181**, 109 (1991).